The Journal of Experimental Biology 211, 2584-2599
Published by The Company of Biologists 2008
doi:10.1242/jeb.018663

Evidence for an apical Na–Cl cotransporter involved in ion uptake in a teleost fish

Junya Hiroi[1,2,*], Shigeki Yasumasu[2], Stephen D. McCormick[3,4], Pung-Pung Hwang[5] and Toyoji Kaneko[6]

[1]Department of Anatomy, St Marianna University School of Medicine, Miyamae-ku, Kawasaki 216-8511, Japan, [2]Department of Materials and Life Sciences, Faculty of Science and Technology, Sophia University, Chiyoda-ku, Tokyo 102-8554, Japan, [3]USGS, Conte Anadromous Fish Research Center, Turners Falls, MA 01376, USA, [4]Department of Biology, University of Massachusetts, Amherst, MA 01003, USA, [5]Institute of Cellular and Organismic Biology, Academia Sinica, Nankang, Taipei 11529, Taiwan, Republic of China and [6]Department of Aquatic Bioscience, Graduate School of Agricultural and Life Sciences, University of Tokyo, Bunkyo-ku, Tokyo 113-8657, Japan

*Author for correspondence (e-mail: j-hiroi@marianna-u.ac.jp)

Accepted 2 June 2008

SUMMARY

Cation–chloride cotransporters, such as the $Na^+/K^+/2Cl^-$ cotransporter (NKCC) and Na^+/Cl^- cotransporter (NCC), are localized to the apical or basolateral plasma membranes of epithelial cells and are involved in active ion absorption or secretion. The objectives of this study were to clone and identify 'freshwater-type' and 'seawater-type' cation–chloride cotransporters of euryhaline Mozambique tilapia (*Oreochromis mossambicus*) and to determine their intracellular localization patterns within mitochondria-rich cells (MRCs). From tilapia gills, we cloned four full-length cDNAs homologous to human cation–chloride cotransporters and designated them as tilapia NKCC1a, NKCC1b, NKCC2 and NCC. Out of the four candidates, the mRNA encoding NKCC1a was highly expressed in the yolk-sac membrane and gills (sites of the MRC localization) of seawater-acclimatized fish, whereas the mRNA encoding NCC was exclusively expressed in the yolk-sac membrane and gills of freshwater-acclimatized fish. We then generated antibodies specific for tilapia NKCC1a and NCC and conducted whole-mount immunofluorescence staining for NKCC1a and NCC, together with Na^+/K^+-ATPase, cystic fibrosis transmembrane conductance regulator (CFTR) and Na^+/H^+ exchanger 3 (NHE3), on the yolk-sac membrane of tilapia embryos acclimatized to freshwater or seawater. The simultaneous quintuple-color immunofluorescence staining allowed us to classify MRCs clearly into four types: types I, II, III and IV. The NKCC1a immunoreactivity was localized to the basolateral membrane of seawater-specific type-IV MRCs, whereas the NCC immunoreactivity was restricted to the apical membrane of freshwater-specific type-II MRCs. Taking account of these data at the level of both mRNA and protein, we deduce that NKCC1a is the seawater-type cotransporter involved in ion secretion by type-IV MRCs and that NCC is the freshwater-type cotransporter involved in ion absorption by type-II MRCs. We propose a novel ion-uptake model by MRCs in freshwater that incorporates apically located NCC. We also reevaluate a traditional ion-uptake model incorporating NHE3; the mRNA was highly expressed in freshwater, and the immunoreactivity was found at the apical membrane of other freshwater-specific MRCs.

Key words: cation–chloride cotransporter, $Na^+/K^+/2Cl^-$ cotransporter, Na^+/Cl^- cotransporter, ion transport, mitochondria-rich cell, chloride cell, tilapia.

INTRODUCTION

Euryhaline teleost fish, such as Mozambique tilapia, *Oreochromis mossambicus*, are able to live in waters with a wide range of salinity and maintain nearly constant ion concentrations of body fluids irrespective of the external salinity. Numerous studies on euryhaline teleosts demonstrate that specialized mitochondria-rich cells (MRCs, also referred to as chloride cells or ionocytes) in the gill epithelium regulate the internal ionic composition, either by secreting excess internal ions in seawater or by taking up needed ions in freshwater (for a review, see Evans et al., 2005). In embryonic and larval stages without functional gills, MRCs have been detected in the epithelia covering the yolk and body, and these extrabranchial MRCs are considered to be the major site of ionic regulation during the early developmental stages (Kaneko et al., 2002; Kaneko and Hiroi, 2008).

In general, epithelial cells are in contact with both the external and internal environments through their apical and basolateral plasma membranes, respectively, and the cells function principally as a physical barrier between the two environments. Furthermore, particular epithelial cells (including fish MRCs) transport ions from the internal to the external environments (i.e. secretion) or from the external to the internal environments (absorption). This vectorial ion transport is performed by combinations of several ion pumps, transporters and channels selectively expressed in each of the apical and basolateral membranes (Jentsch et al., 2004). Therefore, determining the localization patterns of the ion-transport proteins at the apical and basolateral membranes will be essential for determining the ion-transport functions of the cells.

The mechanism of active NaCl secretion by MRCs in seawater-acclimatized fish has been well elucidated, consisting primarily of the cooperative action of three major ion-transport proteins: basolaterally located Na^+/K^+-ATPase, basolaterally located $Na^+/K^+/2Cl^-$ cotransporter (NKCC) and an apically located Cl^- channel homologous to the human cystic fibrosis transmembrane conductance regulator (CFTR) (Silva et al., 1977; Marshall, 2002). However, the ion-uptake mechanism by MRCs in freshwater-acclimatized fish has been controversial over the past 30 years (for reviews, see Marshall, 2002; Perry et al., 2003; Hirose et al., 2003; Evans et al., 2005; Hwang and Lee, 2007). For instance, two models have been proposed for Na^+ uptake at the apical membrane of MRCs in freshwater: the first requires electroneutral

exchange of Na^+ and H^+ by the Na^+/H^+ exchanger (NHE), and the second requires Na^+ absorption through the epithelial Na^+ channel (ENaC), which is electrically coupled with active H^+ excretion by means of the vacuolar-type H^+-ATPase. The former model was proposed originally, and the latter is currently more accepted, but the exact mechanisms of ion uptake by MRCs are still elusive.

Recently, by means of triple immunofluorescence staining for Na^+/K^+-ATPase, NKCC and CFTR, we have ascertained that MRCs in the yolk-sac membrane of seawater-acclimatized tilapia embryos showed the colocalization of basolateral Na^+/K^+-ATPase, basolateral NKCC and apical CFTR (Hiroi et al., 2005), which was completely consistent with the current accepted model for ion secretion by MRCs in seawater. In this study, we unexpectedly encountered another type of MRC, exclusively found in freshwater-acclimatized embryos, which showed basolateral Na^+/K^+-ATPase and apical (and no basolateral) NKCC immunoreactivity. Although the basolateral NKCC immunoreactivity has been found in MRCs of several teleosts (e.g. Pelis et al., 2001; McCormick et al., 2003; Hiroi and McCormick, 2007), the apical NKCC immunoreactivity in the freshwater-exclusive MRCs was surprising: an apical cation–chloride cotransporter has not been suggested previously to be involved in ion uptake in the gills of teleosts. In mammals, however, the $Na^+/K^+/2Cl^-$ cotransporter occurs in two isoforms: NKCC1, a basolaterally located ion-secretory isoform, expressed ubiquitously and especially prominent in ion-secretory epithelial cells, and NKCC2, an apically located ion-absorptive isoform, expressed specifically in the thick ascending limb of the loop of Henle in the kidney (Gamba, 2005). NKCC1 and NKCC2 are members of the cation–chloride cotransporter family, and the family includes the Na^+/Cl^- cotransporter (NCC), which is also an apically located ion-absorptive cotransporter specifically expressed in the distal convoluted tubule in the kidney (Gamba, 2005). In addition, an active ion-uptake model with apical NKCC has been proposed for gills of euryhaline crabs (Riestenpatt et al., 1996; Kirschner, 2004; Luquet et al., 2005). Accordingly, we hypothesized that the differential apical and basolateral localizations of NKCC immunoreactants in freshwater- and seawater-exclusive MRCs, respectively, would represent the existence of the two different cation–chloride cotransporters in tilapia MRCs – 'freshwater-type' (apically located ion-absorptive) and 'seawater-type' (basolaterally located ion-secretory).

An electroneutral, diuretic-sensitive cation–chloride cotransport system was first described in mammalian cells in 1980 (Geck et al., 1980). Since then, various attempts have been made to identify the genes responsible for such a transport system from mammalian cells, mainly because of their pharmacological importance (cation–chloride cotransporters are targets of major diuretics, such as thiazides or loop diuretics), but these have ended in failure (see review by Gamba, 2005). Eventually, a gene encoding NCC was first isolated from winter flounder (*Pseudopleuronectes americanus*) urinary bladder (Gamba et al., 1993), and a gene encoding NKCC1 was cloned from the shark *Squalus acanthias* rectal gland (Xu et al., 1994). The sequence information for these fish genes was subsequently used to 'fish out' the cation–chloride cotransporter family genes from mammalian tissues, and the family, known as the solute carrier family 12 (SLC12), currently consists of nine gene products: NKCC1 (SLC12A2), NKCC2 (SLC12A1), NCC (SLC12A3), four KCCs (SLC12A4, SLC12A5, SLC12A6, SLC12A7) and two orphan members (SLC12A8, SLC12A9) (Hebert et al., 2004; Gamba, 2005). However, little information is yet available on the cation–chloride cotransporter gene family in fish themselves.

The primary goal of this study is to isolate cDNAs of the freshwater- and seawater-type cation–chloride cotransporters from Mozambique tilapia and to demonstrate immunocytochemically the localization patterns of the two cotransporters within MRCs by specific antibodies. We first cloned four tilapia cation–chloride cotransporter homologs. To assess which of the four homologs are most likely the freshwater- and seawater-type cotransporters, we examined the tissue distribution of their mRNAs, as well as time-course changes in their mRNAs, following transfer of tilapia embryos from freshwater to seawater and *vice versa*, by quantitative real-time PCR. Real-time PCR was also performed for the mRNAs of Na^+/H^+ exchanger 3 (NHE3) and vacuolar-type H^+-ATPase, which are the components of the two currently proposed ion-uptake models. Finally, we generated two antibodies distinguishing the freshwater- and seawater-type cotransporters and established quintuple-color immunofluorescence staining for the two cotransporters together with Na^+/K^+-ATPase, CFTR and NHE3, which revealed the localization patterns of the multiple ion-transport proteins at the single-cell level. From the data at both mRNA and protein levels, we were able to identify freshwater- and seawater-type cation–chloride cotransporters in tilapia MRCs.

MATERIALS AND METHODS

Animal and experimental protocol

Mozambique tilapia (*Oreochromis mossambicus* Peters; total length, 15–20 cm) were maintained in tanks with recirculating freshwater (dechlorinated tap water) or 32‰ artificial seawater (Marine Tech, Tokyo, Japan) for 1 month before sampling for RNA extraction. The water was maintained at 25°C and partially replaced once per week, and the fish were fed a commercial goldfish diet daily except for the day of sampling. The fish were anesthetized with 2-phenoxyethanol and decapitated, and the gills, kidney, intestine and brain were immediately excised, cut into small pieces and submerged in RNA*later* RNA Stabilization Reagent (Ambion, Austin, TX, USA).

About 200 fertilized eggs were obtained from the mouth of a brooding female in the freshwater tank immediately after spawning, divided into two groups, preincubated in freshwater or seawater for 4 days, and then freshwater-to-seawater or seawater-to-freshwater transfer was conducted according to our previously published procedure (Hiroi et al., 2005). For RNA extraction, seven embryos were sampled repeatedly 0, 2, 6, 12, 24, 48 and 72 h after transfer. Each embryo was immersed in RNA*later* and the yolk-sac membrane was isolated using sharp-pointed forceps in the reagent. For immunofluorescence staining, five embryos were also sampled repeatedly 0, 24, 48 and 72 h after transfer. The yolk-sac membrane was isolated, fixed in 4% paraformaldehyde in 0.1 mol l^{-1} phosphate buffer (pH 7.4) overnight at 4°C and preserved in 70% ethanol (Hiroi et al., 2005).

Molecular cloning of tilapia NKCC cDNAs by a PCR-based strategy

To obtain cDNA fragments of NKCC homologs, total RNA was isolated from the gills and kidney of freshwater- and seawater-acclimatized tilapia adults using an RNeasy Mini Kit (Qiagen, Valencia, CA, USA), and RT-PCR was performed using a OneStep RT-PCR Kit (Qiagen). Two sets of degenerate primers were designed based on the highly conserved sequences between NKCC1 and NKCC2 of human *Homo sapiens* and shark *Squalus acanthias* [human NKCC1 (GenBank accession no. U30246), human NKCC2 (NM_000338), shark NKCC1 (U05958) and shark NKCC2A (AF521915)]. The primer sequences are as follows: primer set 1

(sense, 5′-ACYTTYGGSCACAACACBRTSGA-3′; antisense, 5′-AARAGCATSACWCCCCADATRTT-3′); primer set 2 (sense, 5′-ATGTTYGTNATHAAYTGGTGGGC-3′; antisense, 5′-CC-NCCRTCRTCRAANARCCACCA-3′). Degenerate positions are represented by the following ambiguity codes: B=C, G, T; D=A, G, T; H=A, C, T; N=A, C, G, T; R=A, G; S=C, G; W=A, T; and Y=C, T. The primer set 1 corresponds to amino acid residues TFGHNTMD (positions 212–219) and NIWGVMLF (298–305) in the human NKCC1 protein, and the primer set 2 corresponds to MFVINWWA (727–734) and WWLFDDGG (1027–1034) in the human NKCC1 protein. PCR amplification was performed by 30 cycles at 94°C for 30 s, at 57°C for 30 s and 72°C for 1 min. The primer set 1 amplified two fragments corresponding to tilapia NKCC1a and tilapia NKCC1b from the tilapia gill RNA, and the primer set 2 amplified a fragment corresponding to tilapia NKCC2 from the tilapia kidney RNA. The PCR products were inserted into pGM-T easy Vector (Promega, Madison, WI, USA) and sequenced using an ABI PRISM 377 DNA Sequencer (Applied Biosystems, Foster City, CA, USA). To obtain full-length DNA sequences of the three fragments, poly(A^+) mRNA was separated from the total RNA of tilapia gills using a mRNA purification kit (Amersham Pharmacia Biotech, Buckinghamshire, UK), and the 5′- and 3′-rapid amplification of cDNA ends (RACE) was performed using a Marathon cDNA amplification kit (Clontech, Mountain View, CA, USA), following the manufacturer's protocol.

Molecular cloning of a tilapia cDNA encoding NCC by immunoscreening with an antibody against human NKCC1

Since none of the three NKCC cDNA clones obtained by the above PCR-based methods seemed likely to correspond to the freshwater-type cotransporter (assessed by the tissue distribution patterns of their mRNAs by real-time PCR), we selected another cloning strategy – immunoscreening of a cDNA expression library. A cDNA expression library was constructed from the freshwater-acclimatized tilapia gill poly(A^+) mRNA by using the ZAP-cDNA Synthesis Kit and the ZAP-cDNA Gigapack III Gold Cloning Kit (Stratagene, La Jolla, CA, USA), following the manufacturer's protocols. Filter transfers of the plated library were screened using a mouse monoclonal antibody directed against the C-terminal 310 amino acids of human NKCC1 (T4, developed by Dr Christian Lytle and Dr Bliss Forbush III, and obtained from the Developmental Studies Hybridoma Bank developed under the auspices of the National Institute of Child Health & Human Development and maintained by The University of Iowa, Department of Biological Sciences, Iowa City, IA, USA). The T4 antibody is known to react with both NKCC1 and NKCC2 (Lytle et al., 1995) and showed immunoreactivity in the apical membrane of MRCs in the gills and embryonic yolk-sac membrane of freshwater-acclimatized tilapia (Wu et al., 2003; Hiroi et al., 2005). One immunopositive clone was isolated in three rounds of plaque purification, and *in vivo* excision of pBluescript SK(–) phagemid was performed from the Uni-ZAP XR vector. The isolated cDNA clone was sequenced.

Sequence analyses

Multiple sequence alignments and phylogenetic analyses were performed using the CLUSTAL W program (Thompson et al., 1994). Prediction of transmembrane segments was performed on the TMHMM Server v. 2.0 (http://www.cbs.dtu.dk/services/TMHMM-2.0). A phylogenetic tree was constructed using the full-length amino acid sequences of tilapia cation–chloride cotransporters, along with those of European eel (*Anguilla anguilla*), zebrafish (*Danio rerio*), medaka (*Oryzias latipes*), winter flounder (*Pseudopleuronectes americanus*), shark (*Squalus acanthias*) and human (*Homo sapiens*), according to the neighbor-joining method (Saitou and Nei, 1987). The human K^+/Cl^- cotransporter (KCC1, SLC12A4) was used as an outgroup. The full-length amino acid sequences of three zebrafish NCC homologs and three medaka NCC homologs were retrieved from the Ensembl website (http://www.ensembl.org) or from the medaka genome database (golw_scaffold Hd-rR 200506, http://dolphin.lab.nig.ac.jp/medaka) and tentatively named zebrafish NCCa, zebrafish NCCb, zebrafish NCCc, medaka NCCa, medaka NCCb and medaka NCCc, respectively. All other sequences were obtained from the NCBI Genbank database (http://www.ncbi.nlm.nih.gov). The reliability of the tree was assessed by a bootstrap analysis with 1000 replicates (Felsenstein, 1985).

Quantitative real-time PCR

The mRNA levels of tilapia NKCC1a, tilapia NKCC1b, tilapia NKCC2, tilapia NCC, tilapia NHE3 and tilapia H^+-ATPase were determined by using quantitative real-time PCR. Total RNA was isolated from each of the RNA*later*-treated tissues using an RNeasy Mini Kit (30 mg of adult tissue or whole yolk-sac membrane of a single embryo was processed individually with an RNeasy mini column), and cDNA was synthesized in a 5 µl reaction using the total RNA (0.25 µg for adult tissue or 3 µl for yolk-sac membrane) and the QuantiTect Reverse Transcription Kit with genomic DNA wipeout buffer (Qiagen). Real-time PCR was performed by an ABI PRISM 7000 Sequence Detection System (Applied Biosystems) in a 20 µl reaction using 2 µl of the 1:10-diluted cDNA, 300 nmol l^{-1} of primers and 10 µl of Power SYBR Green PCR Master Mix (Applied Biosystems). The primer sequences are shown in Table 1. Gene-specific primers for tilapia NKCC1a, NKCC1b, NKCC2, NCC and 18S rRNA were designed using Primer Express software (Applied Biosystems). Each of the primers for the four tilapia cation–chloride cotransporters was designed not to amplify other cotransporters and was designed to span putative exon–intron boundaries to avoid amplification of genomic DNA. As the exon–intron organization is highly conserved among NKCC1, NKCC2 and NCC in human (examined on the Ensembl website), the boundaries of human cotransporters were used to predict those of tilapia. Only for NKCC1b were we unable to design primers

Table 1. Primers used for quantitative real-time PCR

Tilapia gene	GenBank accession no.	Sense (5′ to 3′)	Antisense (5′ to 3′)	Product size (bp)
NKCC1a	AY513737	GGAGGCAAGATCAACAGGATTG	AATGTCCGAAAAGTCTATCCTGAACT	84
NKCC1b	AY513738	AGAACTTTGGTCCAGAATTCAGAGAT	CCAGTAGCTGCAGGGAAGAAA	76
NKCC2	AY513739	CTCATCGGTGACCTCAACAC	CAACCTGGAGATTTGGCATA	113
NCC	EU518934	CCGAAAGGCACCCTAATGG	CTACACTTGCACCAGAAGTGACAA	79
NHE3	AB326212	AAGCGGCACCCATCACTACA	GAGCCAGCAAACCAGAATCCA	98
H^+-ATPase	AB369668	CCACAGCTCAGAGCGACAACA	GCATACTCGGCCTTGATCTTG	136
18S rRNA	AF497908	CGGAGAGGGAGCCTGAGAA	AGTCGGGAGTGGGTAATTTGC	73

spanning exon–intron boundaries with high amplification efficiency. The primers for NHE3 and the vacuolar-type H^+-ATPase A-subunit were designed by M. Inokuchi and K. M. Lee. The reaction conditions were 95°C for 10 min to activate polymerase, followed by 40 cycles at 95°C for 15 s and at 60°C for 1 min. Amplification was followed by a melting-curve analysis to confirm the specificity of the PCR reaction. The relative levels of each mRNA were normalized to the corresponding 18S rRNA levels because 18S rRNA was stably expressed in all examined adult tissues (P=0.16, one-way ANOVA) and in embryonic yolk-sac membrane during the transfer experiments (freshwater-to-seawater transfer, P=0.30; seawater-to-freshwater transfer, P=0.83).

Antibodies

To detect tilapia NKCC1a and tilapia NCC immunocytochemically, rabbit polyclonal antisera were raised against synthetic peptides corresponding to the amino terminal sequences of tilapia NKCC1a (MSAPSSASSAPAEN) and tilapia NCC (MGQFNSKNKGSGPGI) and were purified by affinity chromatography (Operon Biotechnologies, Tokyo, Japan). The specificity of antisera against NKCC1a and NCC was assessed by western blot analysis with freshwater- and seawater-acclimatized tilapia gills, according to the method described previously (Hiroi and McCormick, 2007). The anti-NKCC1a detected an expected 150 kDa band in the gills of seawater fish (Fig. 1A). No distinct band was detected with the antiserum against NCC (Fig. 1B), indicating that this antibody does not work under the denaturing conditions of western blotting. The specificity of antiserum against NCC was then confirmed by a preabsorption test in indirect immunofluorescence staining: the NCC-positive immunoreactivity in the yolk-sac membrane of freshwater-acclimatized embryos (Fig. 1C) was completely abolished by preabsorbing the antiserum against NCC (4.5 μg ml^{-1}) with the corresponding antigen peptide (1 μg ml^{-1}) for 1 h at 37°C (Fig. 1D).

Na^+/K^+-ATPase was detected by an affinity-purified rabbit polyclonal antibody directed against a synthetic peptide corresponding to part of the highly conserved region of the Na^+/K^+-ATPase α-subunit (VTGVEEGRLIFDNLKKS) (Katoh et al., 2000). NHE3 was detected by an affinity-purified rabbit polyclonal antibody directed against a synthetic peptide corresponding to part of the carboxyl-terminal region of tilapia NHE3 (TDTKQMNNDQFPPP) (Watanabe et al., 2008). CFTR was detected by a protein-G-purified mouse monoclonal antibody against 104 amino acids at the carboxyl-terminus of human CFTR (R&D Systems, Boston, MA, USA), which has been shown to detect CFTR in several teleosts (Marshall et al., 2002; McCormick et al., 2003; Wilson et al., 2004; Hiroi et al., 2005). The specificity of antisera against Na^+/K^+-ATPase, NHE3 and CFTR has already been confirmed by western blot analysis in previous studies (Katoh et al., 2000; Marshall et al., 2002; Katoh and Kaneko, 2003; Watanabe et al., in press).

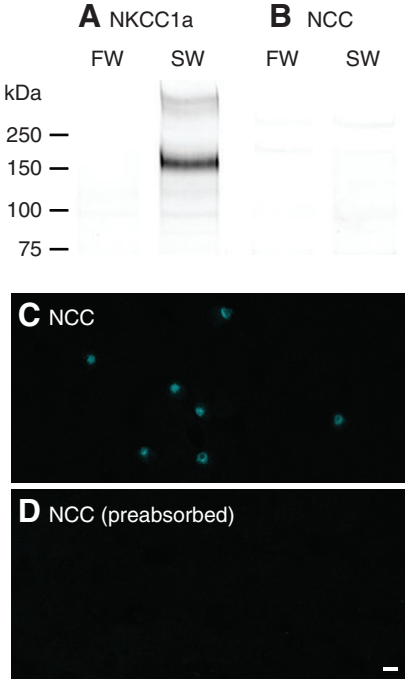

Fig. 1. Western blot analysis of (A) NKCC1a and (B) NCC in the gills of Mozambique tilapia acclimatized to freshwater (FW) or seawater (SW), and (C,D) a preabsorption test for NCC immunofluorescence staining in the yolk-sac membrane of freshwater-acclimatized tilapia embryos. The NCC-positive immunoreactivity (C) is completely abolished by preabsorbing antibody against NCC with the corresponding antigen peptide (D). Molecular mass standards are indicated (kDa). Scale bar, 10 μm.

To allow quintuple-color immunofluorescence staining for Na^+/K^+-ATPase, NKCC1a, NCC, NHE3 and CFTR, each of the five antibodies was directly labeled with Alexa Fluor dyes using Zenon antibody labeling kits (Molecular Probes, Eugene, OR, USA). The dyes were assigned to each antibody as follows: anti-Na^+/K^+-ATPase, Alexa Fluor 488; anti-NKCC1a, Alexa Fluor 430; anti-NCC, Alexa 405; anti-NHE3, Alexa Fluor 555; and anti-CFTR, Alexa Fluor 647. The wavelengths of maximum excitation and emission of each Alexa Fluor dye are shown in Table 2. Before quintuple-color immunofluorescence staining, conventional single-color indirect immunofluorescence staining with Alexa-Fluor-conjugated secondary antibodies was carried out for each of the primary antibodies, resulting in the same staining patterns as the quintuple-color staining. Negative-control experiments (without primary antibody) showed no specific staining.

Table 2. Alexa Fluor dyes used to label antibodies against Na^+/K^+-ATPase, NKCC1a, NCC, NHE3 and CFTR

	Alexa Fluor	Ex/Em* (nm)	Ex/Em† (nm)	Pseudocolor
Na^+/K^+-ATPase	488	495/519	488/505-530	Red
NKCC1a	430	434/539	405/>530	Blue
NCC	405	402/421	405/420-480	Cyan
NHE3	555	555/565	543/560-615	Yellow
CFTR	647	650/668	633/>650	Green

*Wavelength of maximum excitation and emission of each Alexa Fluor dye. †Wavelength of laser excitation and recorded emission for confocal laser-scanning microscopy.

Quintuple-color whole-mount immunofluorescence staining

The fixed embryonic yolk-sac membrane was permeabilized in 0.01 mol l^{-1} phosphate-buffered saline containing 0.2% Triton X-100 (PBST, pH 7.2) for 1 h at room temperature, incubated with Image-iT FX Signal Enhancer (Molecular Probes) for 30 min at room temperature and then incubated simultaneously with Alexa-Fluor-labeled antibodies against Na^+/K^+-ATPase (1.7 μg ml^{-1}), NKCC1a (11 μg ml^{-1}), NCC

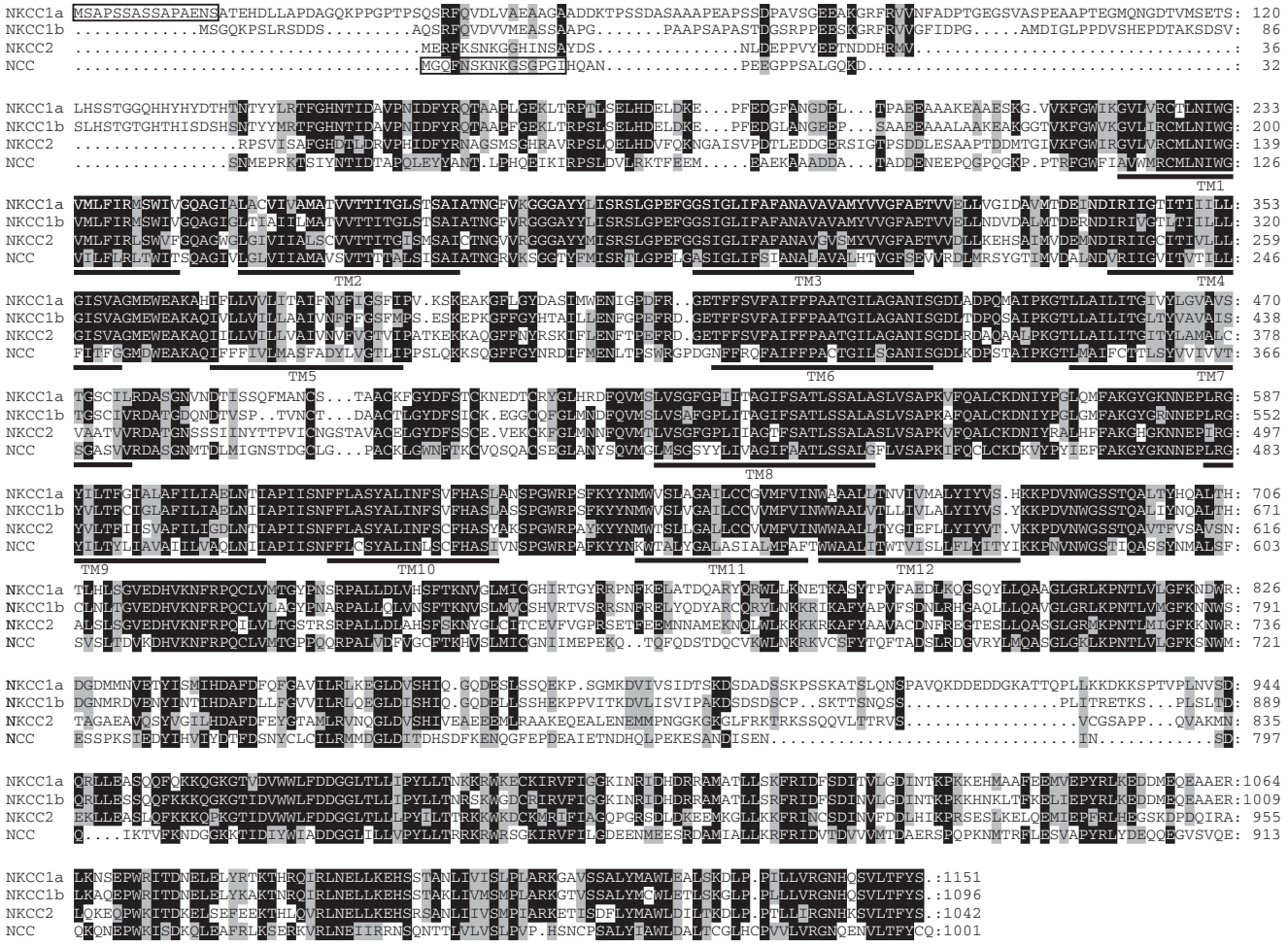

Fig. 2. Multiple alignment of the deduced amino acid sequence of tilapia NKCC1a (GenBank accession no. AY513737), tilapia NKCC1b (AY513738), tilapia NKCC2 (AY513739) and tilapia NCC (EU518934) cDNAs that were isolated from the gills of Mozambique tilapia. Conserved and similar amino acids are shaded in black and gray, respectively. Putative transmembrane segments are underlined (TM1–TM12). The boxed amino-terminal sequences of tilapia NKCC1a and tilapia NCC were used as antigens to produce antibodies against tilapia NKCC1a and tilapia NCC.

(4.5 μg ml^{-1}), NHE3 (7.7 μg ml^{-1}) and CFTR (1 μg ml^{-1}) for 12 h at 10°C under gentle agitation. The antibodies were diluted with PBST containing 0.02% keyhole limpet hemocyanin, 0.1% bovine serum albumin, 10% normal goat serum and 0.01% sodium azide. The membrane was washed in PBST for 1 h, subjected to post-staining fixation with 4% paraformaldehyde for 15 min, washed briefly in PBST and mounted under a coverslip using Prolong Gold Antifade Reagent (Molecular Probes).

The region of the yolk-sac membrane close to the embryonic body was examined under a Carl Zeiss LSM510 confocal laser-scanning microscope equipped with a C-apochromat 40×, numerical aperture 1.2, water-immersion lens. The wavelengths of laser excitation and recorded emission for each Alexa Fluor dye are shown in Table 2. Confocal pinholes were set to allow 1 μm optical sections separately for each dye, and confocal images were taken at 0.5 μm intervals to generate Z-stacks. Images were pseudocolored using image-processing software (Adobe Photoshop 7.0, San Jose, CA, USA), mainly according to the pseudocoloring described in our previously published study (Hiroi et al., 2005), irrespective of the original emission spectra of the dyes (Table 2). The image size was 0.053 mm^2, and at least 10 images were obtained from each embryo in order to count the number of each MRC type.

Solution to a fluorescence crosstalk problem

Each signal of Alexa Fluor 488, Alexa Fluor 405, Alexa Fluor 555 and Alexa Fluor 647 was well separated, with little crosstalk. By contrast, Alexa Fluor 430, which has a large stokes shift and relatively broad excitation and emission spectra, resulted in a slight crosstalk with the setting for Alexa Fluor 488. However, the crosstalk was negligible by assigning Alexa Fluor 430 to the antibody against NKCC1a, and assigning Alexa Fluor 488 to the antibody against Na^+/K^+-ATPase, for the following two reasons. First, the antibody against Na^+/K^+-ATPase usually showed much stronger immunoreactivity than antibody against NKCC1a, and consequently the crosstalk of Alexa Fluor 430 for antibody against NKCC1a was relatively much weaker than the signal of Alexa Fluor 488 for antibody against Na^+/K^+-ATPase. Second, NKCC1a-positive cells were always known to be a subset of Na^+/K^+-ATPase-positive cells, and the two antibodies showed an almost equivalent basolateral staining pattern within the cell, so that the crosstalk of Alexa Fluor 430 for antibody against NKCC1a should hardly affect the staining

pattern of Alexa-Fluor-488-labeled antibody against Na^+/K^+-ATPase.

Statistics

The temporal changes in the mRNA levels for NKCC1a, NCC, NHE3 and H^+-ATPase were analyzed by one-way analysis of variance (ANOVA) and a Tukey–Kramer *post-hoc* test. Before analysis, data displaying heterogeneity of variances were log-transformed by $X'=\log_{10}(X+1)$ (Zar, 1999). As the ANOVA and *post-hoc* test were repeated four times for four genes, the P value was lowered from the widely used 0.05 to 0.0125 (=0.05/4) to avoid excessive type-I errors. The temporal changes in the number of four MRC types were also analyzed by one-way ANOVA and Tukey–Kramer *post-hoc* test, with the P value of 0.0125 (=0.05/4), as the tests were repeated four times for four MRC types. All analyses were conducted using JMP 5.0.1 (SAS Institute, Cary, NC, USA).

RESULTS

Four cation–chloride cotransporters isolated from tilapia gills

From the gills of Mozambique tilapia, three full-length cDNAs homologous to human NKCC were obtained by the PCR-based strategy, and one full-length cDNA homologous to human NCC rather than NKCC was isolated by immunoscreening using antibody against human NKCC1. These four cDNAs exhibited open reading frames encoding proteins of 1001 to 1151 amino acids (Fig. 2). In this study, the former three NKCC homologs were designated as tilapia NKCC1a (GenBank accession no. AY513737), tilapia NKCC1b (AY513738) and tilapia NKCC2 (AY513739), and the latter NCC homolog was designated as tilapia NCC (EU518934), according to their amino acid identities to human NKCC1, NKCC2 and NCC, respectively, as follows: tilapia NKCC1a, 69.1%, 56.4% and 43.5%; tilapia NKCC1b, 63.9%, 57.5% and 44%; tilapia NKCC2, 49.8%, 60.8% and 43.9%; tilapia NCC, 39.4%, 42.3% and 52.1%. In all the four tilapia homologs, twelve transmembrane segments were predicted (underlined sequences in Fig. 2), which are a characteristic of the cation–chloride cotransporter family (Gerelsaikhan and Turner, 2000; Gamba 2005). Among the four tilapia homologs, the transmembrane segments and the carboxyl-terminus showed high homology, whereas the amino terminus was the most divergent. Therefore, the amino-terminal sequences of tilapia NKCC1a and tilapia NCC were used as antigens to produce antibodies in rabbits (boxed sequences in Fig. 2).

In a phylogenetic tree constructed by the neighbor-joining method (Fig. 3), all examined cotransporters were first divided into two major clades, the NKCC clade and the NCC clade. The NKCC clade was further divided into two – the NKCC1 clade and the NKCC2 clade. Tilapia NKCC1a and tilapia NKCC1b were assigned to the NKCC1 clade, and tilapia NKCC2 was assigned to the NKCC2 clade. The NCC clade was also divided into two clades. One clade consisted of eel NCCα, zebrafish NCCa, medaka NCCa, flounder NCC and human NCC, and was named the conventional NCC clade. Another clade consisted of eel NCCβ, zebrafish zNCCg, zebrafish NCCb, zebrafish NCCc, medaka NCCb and medaka NCCc, and was named the fish-specific NCC clade. Tilapia NCC was assigned to the fish-specific NCC clade.

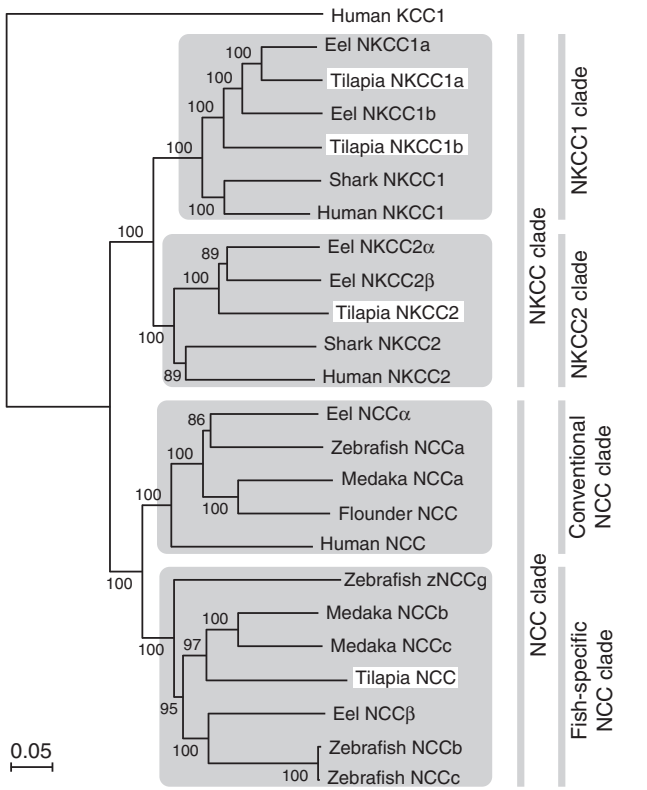

Fig. 3. A phylogenetic tree of full-length amino acid sequences of fish and human cation–chloride cotransporters, constructed by the neighbor-joining method. Tilapia NKCC1a, NKCC1b, NKCC2 and NCC are highlighted. Human K^+/Cl^- cotransporter (KCC1) was used as an outgroup to root the tree. The sequences were grouped into four clades (NKCC1 clade, NKCC2 clade, conventional NCC clade and fish-specific NCC clade). Numbers at the nodes are the bootstrap values for 1000 replications, shown as percentages. Bar, evolutionary distance of 0.05 amino acid substitution per site. The GenBank accession numbers are as follows: tilapia (NKCC1a, AY513737; NKCC1b, AY513738; NKCC2, AY513739; NCC, EU518934), eel (NKCC1a, AJ486858; NKCC1b, AJ486859; NKCC2α, AJ564602; NKCC2β, AJ564603; NCCα, AJ564604; NCCβ, AJ564606), zebrafish (zNCCg, EF591989; NCCa, NP_001038545; NCCb, XP_001342888; NCCc, XP_699464), medaka (NCCa, Ensembl protein report for ENSORLP00000000509; NCCb, ENSORLP00000023616; NCCc, scaffold1460 of golw_scaffold Hd-rR 200506), flounder (NCC, L11615), shark (NKCC1, U05958; NKCC2, AF521915) and human (NKCC1, U30246; NKCC2, NM_000338; NCC, X91220; KCC1, NM_005072).

Tissue distribution of mRNAs for NKCC1a, NKCC1b, NKCC2, NCC, NHE3 and H^+-ATPase

Each of the four tilapia cation–chloride cotransporter mRNAs showed distinct tissue distribution patterns (Fig. 4A–D). The mRNA encoding NKCC1a was detectable in all tissues examined and was highly expressed in the yolk-sac membrane and gills of seawater-acclimatized fish (Fig. 4A). The NKCC1b mRNA was the highest in the brain, whereas the NKCC2 mRNA was the highest in the intestine and less, but still notable, in the kidney, in both freshwater- and seawater-acclimatized fish (Fig. 4B,C). The mRNA encoding NCC was highly expressed in the yolk-sac membrane and gills in freshwater-acclimatized fish and was not detectable (below 0.1% of the value of freshwater gills) in other tissues (Fig. 4D). The NHE3 mRNA was expressed noticeably in the yolk-sac membrane, gills and kidney, in which the expression was higher in freshwater fish than in seawater fish (Fig. 4E). The mRNA encoding H^+-ATPase A-subunit was detectable in all tissues and highly expressed in the brain (Fig. 4F).

Temporal changes in mRNA levels for NKCC1a, NCC, NHE3 and H^+-ATPase during transfer experiments

The temporal changes in the yolk-sac mRNA levels following transfer of tilapia embryos from freshwater to seawater are shown

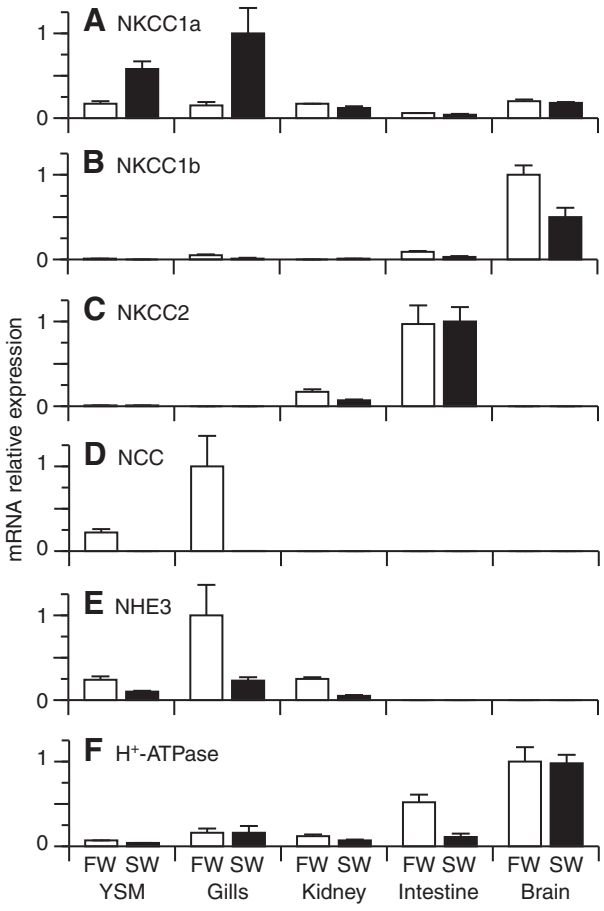

Fig. 4. Tissue distribution of mRNAs encoding (A) NKCC1a, (B) NKCC1b, (C) NKCC2, (D) NCC, (E) NHE3 and (F) vacuolar-type H^+-ATPase A-subunit in Mozambique tilapia acclimatized to freshwater (FW) and seawater (SW), quantified using real-time PCR. The yolk-sac membrane of embryos 4 days after fertilization (YSM), adult gills, kidney, intestine and brain were examined. Each value represents the mean ± s.e.m., *N*=7 (YSM) and *N*=3 (adult tissues). The data were normalized to the highest-expressing tissue for each gene, which were assigned an arbitrary value of 1.

in Fig. 5A. One-way ANOVA revealed a significant effect of time on NKCC1a (P=0.0002) and NCC (P<0.0001) but not on NHE3 (P=0.14) and H^+-ATPase A-subunit (P=0.17). The NKCC1a mRNA was relatively low at 0 h, increased threefold within 6 h and remained high through 72 h (P<0.0125 between 0 h and 6–72 h, Tukey–Kramer test). By contrast, the NCC mRNA was relatively high at 0 h, decreased to one-tenth at 12 h and remained low through 72 h (P<0.0125 between 0–6 h and 12–72 h).

The temporal changes in the yolk-sac mRNA levels following transfer from seawater to freshwater are shown in Fig. 5B. Significant changes were observed in NKCC1a (P<0.0001, one-way ANOVA), NCC (P<0.0001) and NHE3 (P<0.0001), but were not observed in the H^+-ATPase A-subunit (P=0.03). Yolk-sac NKCC1a mRNA was high at 0 h, decreased gradually to one-third at 24 h and remained at that level through 72 h (P<0.0125 between 0 h and 12–72 h, Tukey–Kramer test). NCC mRNA was extremely low at 0 h, increased gradually but significantly after transfer and reached the highest level at 72 h (P<0.0125 between 0–2 h and 48–72 h). NHE3 mRNA was relatively low at 0 h, increased to reach a peak at 24 h (sevenfold increase compared with the initial level) and thereafter fluctuated but remained high (P<0.0125 between 0–6 h and 24 h, and between 0–6 h and 72 h).

Classification of MRCs into four types

During transfer of tilapia embryos from freshwater to seawater and *vice versa*, MRCs in the yolk-sac membrane could be clearly classified into four types (Table 3, Fig. 6), according to the staining patterns for Na^+/K^+-ATPase, NKCC1a, NCC and CFTR: type I, showing only basolateral Na^+/K^+-ATPase staining (Fig. 6A); type II, basolateral Na^+/K^+-ATPase and apical NCC (Fig. 6B); type III, basolateral Na^+/K^+-ATPase and basolateral NKCC1a (Fig. 6C); type IV, basolateral Na^+/K^+-ATPase, basolateral NKCC1a and apical CFTR (Fig. 6D).

The immunoreactivity for Na^+/K^+-ATPase and NKCC1a was detectable throughout the MRC except for the nucleus and the apical region (Na^+/K^+-ATPase and NKCC1a in Fig. 6). This staining pattern of Na^+/K^+-ATPase and NKCC1a within MRCs was regarded as representing a basolateral distribution (Table 3) as the basolateral membrane of MRCs is known to be invaginated to form an extensive tubular system throughout the whole cytoplasm (Evans et al., 2005). By contrast, the immunoreactivity for NCC, NHE3 and CFTR was shown to be restricted to the apical region of types II, III and IV, respectively, by changing the depth of focus to reconstruct *X*–*Z*-plane images (merged *X*–*Z* plane in Fig. 6; Table 3). The immunoreactivity for the five ion-transport proteins was restricted to MRCs and negligible in other cells (e.g. respiratory pavement cells and undifferentiated cells).

The NCC-positive apical region in type-II MRCs showed a variation in morphology during the transfer experiments. In embryos in freshwater, the apical NCC immunoreactivity was relatively small (1–2 μm in diameter, Fig. 7A,C), but the apical region was in contact with the external environment (Fig. 7E, a distinct apical opening of a type-II MRC was observed by differential-interference-contrast microscopy). In embryos at 72 h following transfer from freshwater to seawater, the apical NCC immunoreactivity was still evident (Fig. 7H,J), but the apical opening was not obvious and was covered with surface pavement cells (Fig. 7L). In embryos transferred from seawater to freshwater, the apical NCC immunoreactivity was faint at 24 h (Fig. 7O,Q) but showed a large cup-like appearance (3–5 μm in diameter, Fig. 7V–X) or a wide and shallow opening (8–14 μm in diameter, Fig. 7AC–AE) at 48 h and 72 h.

The apical NHE3 immunoreactivity was detectable only in type-III MRCs in embryos at 0 h of freshwater-to-seawater transfer, and at 72 h of seawater-to-freshwater transfer, but the staining intensity was relatively low compared with the apical immunoreactivity of NCC (type-II MRCs) or CFTR (type-IV MRCs); the apical NHE3 immunoreactivity was distinct in some type-III MRCs but often very weak and not distinguishable from background levels in other type-III MRCs.

Temporal changes in the number of four types of MRCs during transfer experiments

In embryos in freshwater (at 0 h of freshwater-to-seawater transfer), type-I, type-II and type-III MRCs were observed (Fig. 8A–F), and the proportions were as follows: type I, 30%; type II, 17%; type III, 53%; type IV, 0%. The temporal changes in the density of each MRC type following transfer from freshwater to seawater are shown in Fig. 9A. One-way ANOVA revealed a significant effect of salinity on the number of type-II MRCs (P=0.0004), type-III MRCs (P<0.0001) and type-IV MRCs (P<0.0001) but not on type-I MRCs (P=0.84). Type-II MRCs decreased in number significantly (P<0.0125 between 0 h and 48–72 h, Tukey–Kramer test). Type-III

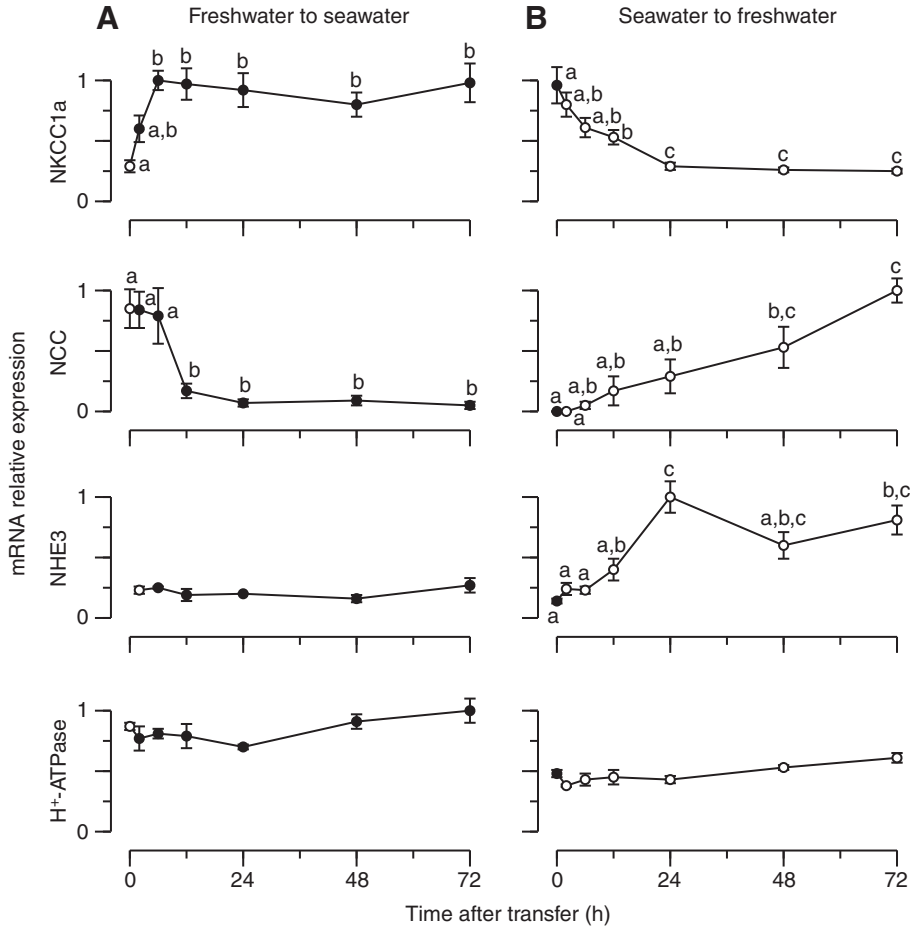

Fig. 5. Changes in the levels of mRNA encoding NKCC1a, NCC, NHE3 and the H^+-ATPase A-subunit following transfer of Mozambique tilapia embryos from (A) freshwater to seawater and (B) *vice versa*, quantified using real-time PCR. Each value represents the mean ± s.e.m., N=7. The data from both transfer experiments (which were conducted simultaneously and assays run at the same time) were normalized to the highest value for each gene (NKCC1a, at 6 h of freshwater-to-seawater transfer; NCC, at 72 h of seawater-to-freshwater transfer; NHE3, at 24 h of seawater-to-freshwater transfer; H^+-ATPase, at 72 h of freshwater-to-seawater transfer), which were assigned an arbitrary value of 1. The data at 0 h were derived from the same samples as used in Fig. 4. Unfilled circles, values in freshwater; filled circles, values in seawater. Values with different lowercase letters are significantly different (e.g. a significant difference is observed between 'a' and 'b', but not between 'a' and 'a,b', or between 'b' and 'a,b'; P<0.0125, Tukey–Kramer test).

MRCs decreased rapidly in number and almost disappeared by 48 h (P<0.0125 between 0 h and 24–72 h), and conversely type-IV MRCs appeared and rapidly increased in number (P<0.0125 between 0 h and 24–72 h). Consequently, at 72 h after transfer from freshwater to seawater, type I, type II and type IV were mainly observed (Fig. 8G–L), and the ratio was as follows: type I, 34%; type II, 4%; type III, 1%; type IV, 62%.

In embryos in seawater (at 0 h of seawater-to-freshwater transfer), type-I, type-III and type-IV MRCs were observed (Fig. 8M–R), and the proportions were as follows: type I, 23%; type II, 0%; type III, 9%; type IV, 68%. The temporal changes in the density of each MRC type following transfer from seawater to freshwater are shown in Fig. 9B. One-way ANOVA revealed a significant effect of freshwater on the number of type-II MRCs (P=0.0005), type-III MRCs (P<0.0001) and type-IV MRCs (P<0.0001) but not on type-I MRCs (P=0.94). Type-II MRCs were not found at 0 h, started to appear at 24 h (detectable in one out of five embryos) and increased in number after that (P<0.0125 between 0 h and 72 h, Tukey–Kramer test). Type-III MRCs rapidly increased in number (P<0.0125 between 0 h and 24–72 h), and conversely type-IV MRCs rapidly decreased and almost disappeared by 48 h (P<0.0125 between 0 h and 24–72 h). Consequently, at 72 h after transfer from seawater to freshwater, type I, type II and type III were observed (Fig. 8S–X), and the ratio was: type I, 28%; type II, 26%; type III, 46%; type IV, 0%.

DISCUSSION

Identification of freshwater- and seawater-type cotransporters

The first objective of this study was to identify the genes of 'freshwater-type' and 'seawater-type' cation–chloride cotransporters in tilapia MRCs by molecular cloning and real-time PCR mRNA quantification. From tilapia gills, we isolated four cation–chloride cotransporter homologs and designated them as tilapia NKCC1a, NKCC1b, NKCC2 and NCC (Figs 2 and 3). Of the four candidates, the NKCC1a mRNA was highly expressed in the yolk-sac membrane and gills of seawater-acclimatized fish (Fig. 4A), and the mRNA in the yolk-sac membrane was upregulated in seawater and downregulated in freshwater during transfer experiments with embryos (Fig. 5); conversely, the NCC mRNA was expressed only in the yolk-sac membrane and gills of freshwater-acclimatized fish (Fig. 4D), and the mRNA was downregulated in seawater and

Table 3. Classification of four types of mitochondria-rich cells in the yolk-sac membrane of Mozambique tilapia embryos, defined by immunofluorescence patterns for Na^+/K^+-ATPase, NKCC1a, NCC, NHE3 and CFTR

	Type I	Type II	Type III	Type IV
Na^+/K^+-ATPase	Basolateral	Basolateral	Basolateral	Basolateral
NKCC1a	–	–	Basolateral	Basolateral
NCC	–	Apical	–	–
NHE3	–	–	Apical or –	–
CFTR	–	–	–	Apical

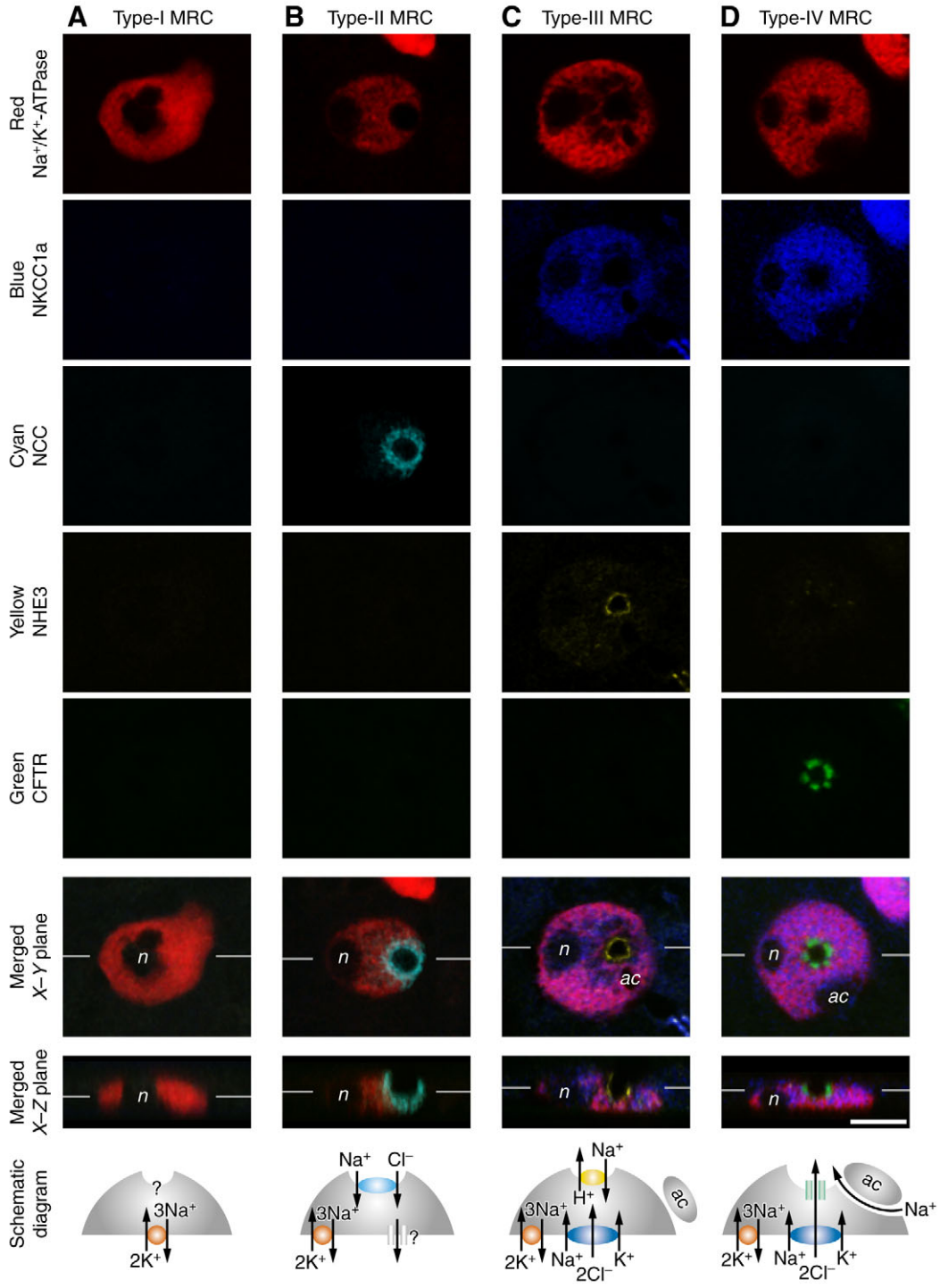

Fig. 6. Classification of mitochondria-rich cells (MRCs) in the yolk-sac membrane of Mozambique tilapia embryos into four types by means of quintuple-color immunofluorescence staining: (A) type-I MRC (at 72 h of seawater-to-freshwater transfer), (B) type-II MRC (at 72 h of seawater-to-freshwater transfer), (C) type-III MRC (at 72 h of seawater-to-freshwater transfer) and (D) type-IV MRC (at 72 h of freshwater-to-seawater transfer). The immunofluorescence signals for Na^+/K^+-ATPase (red), NKCC1a (blue), NCC (cyan), NHE3 (yellow) and CFTR (green) are shown as separate channels, and the five channels are merged in Merged *X–Y* and *X–Z* planes. Merged *X–Z* plane, the *X–Z* optical section cut transversely at the horizontal lines indicated in Merged *X–Y* plane. Merged *X–Y* plane, the *X–Y* optical section cut at the lines indicated in Merged *X–Z* plane. *n*, nucleus; *ac*, accessory cell. Scale bar, 10 μm. Schematic diagrams of each of the four cell types are presented in the bottom row, showing the apical or basolateral localization patterns of Na^+/K^+-ATPase (red), NKCC1a (blue), NCC (cyan), NHE3 (yellow) and CFTR (green).

upregulated in freshwater (Fig. 5). These high expression levels of NKCC1a and NCC in the yolk-sac membrane and gills, which are the sites of the MRC localization, imply that they are expressed in MRCs, and their expression preference for seawater or freshwater clearly substantiates that NKCC1a is the 'seawater-type' cotransporter involved in ion secretion and that NCC is the 'freshwater-type' cotransporter involved in ion absorption. These speculations based on the mRNA data were also supported by the immunocytochemical data, which will be discussed in the section below.

From tilapia gills, we cloned cDNAs encoding two NKCC1 (NKCC1a and NKCC1b), one NKCC2 and one NCC protein (Figs 2 and 3). By contrast, in the European eel *Anguilla anguilla*, cDNAs encoding two NKCC1 (NKCC1a and NKCC1b), two NKCC2 (NKCC2α and NKCC2β) and two NCC (NCCα and NCCβ) proteins were comprehensively cloned from various tissues (Cutler and Cramb, 2002; Cutler and Cramb, 2008). It was suggested that the presence of these duplicate pairs of eel NKCC1, NKCC2 and NCC isoforms might reflect a whole-genome duplication event in the teleost ancestor (Cutler and Cramb, 2002; Cutler and Cramb,

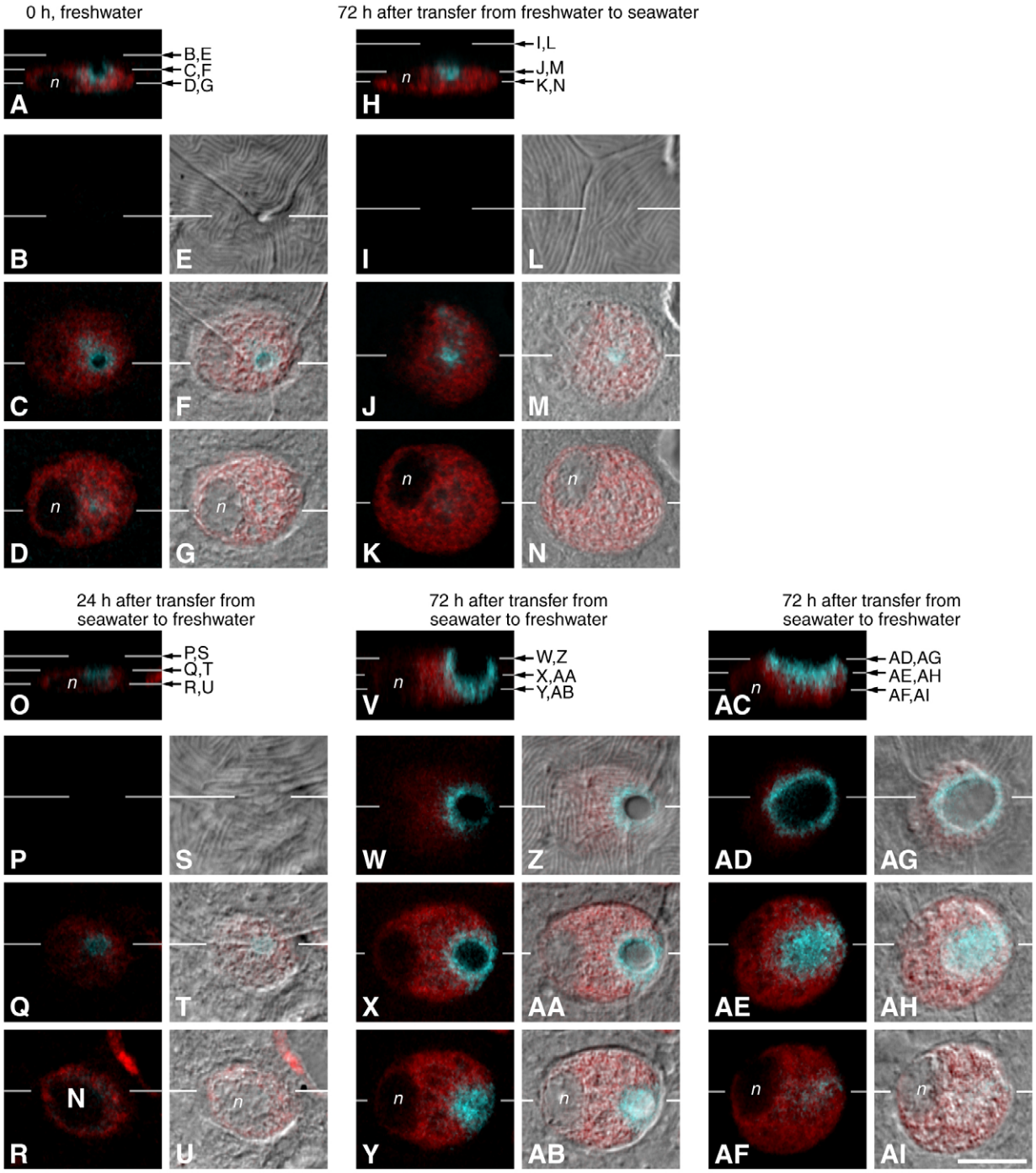

Fig. 7. Variation in type-II mitochondria-rich cell morphology: (A–G) a cell with a relatively small apical opening in an embryo in freshwater (at 0 h of freshwater-to-seawater transfer); (H–N) a remaining cell in an embryo transferred from freshwater to seawater (at 72 h of freshwater-to-seawater transfer); (O–U) a newly appearing cell in an embryo transferred from seawater to freshwater (at 24 h of seawater-to-freshwater transfer); cells with (V–AB) a deep apical opening and with (AC–AI) a wide apical opening in an embryo transferred from seawater to freshwater (at 72 h of seawater-to-freshwater transfer). (A,H,O,V,AC) *X–Z* optical sections, cut at the lines indicated in *X–Y* optical sections. (B–D,I–K,P–R,W–Y,AD–AF) *X–Y* optical sections, cut at three different lines indicated in *X–Z* optical sections: the focus is placed in the outer surface plane of the yolk-sac membrane (B,I,P,W,AD), in the plane through the center of the NCC immunoreactivity (C,J,Q,X,AE) and in the plane through the center of the nucleus (D,K,R,Y,AF). Channels for Na^+/K^+-ATPase (red) and NCC (cyan) are merged in A–D, H–K, O–R, V–Y and AC–AF. The merged *X–Y* images are further merged with corresponding differential-interference-contrast images (E–G,L–N,S–U,Z–AB,AG–AI). *n*, nucleus. Scale bar, 10 μm.

2008), which has been estimated by comparison with human and teleost genomes (Kasahara et al., 2007). Therefore, it is possible that other isoforms of NKCC2 and/or NCC are present in other tissues of tilapia.

The mRNAs of tilapia NKCC1a and NKCC1b were expressed highly in the gills (in seawater) and brain (both freshwater and seawater), respectively (Fig. 4A,B), which is consistent with data from eel NKCC1a and NKCC1b (Cutler and Cramb, 2002). Tilapia

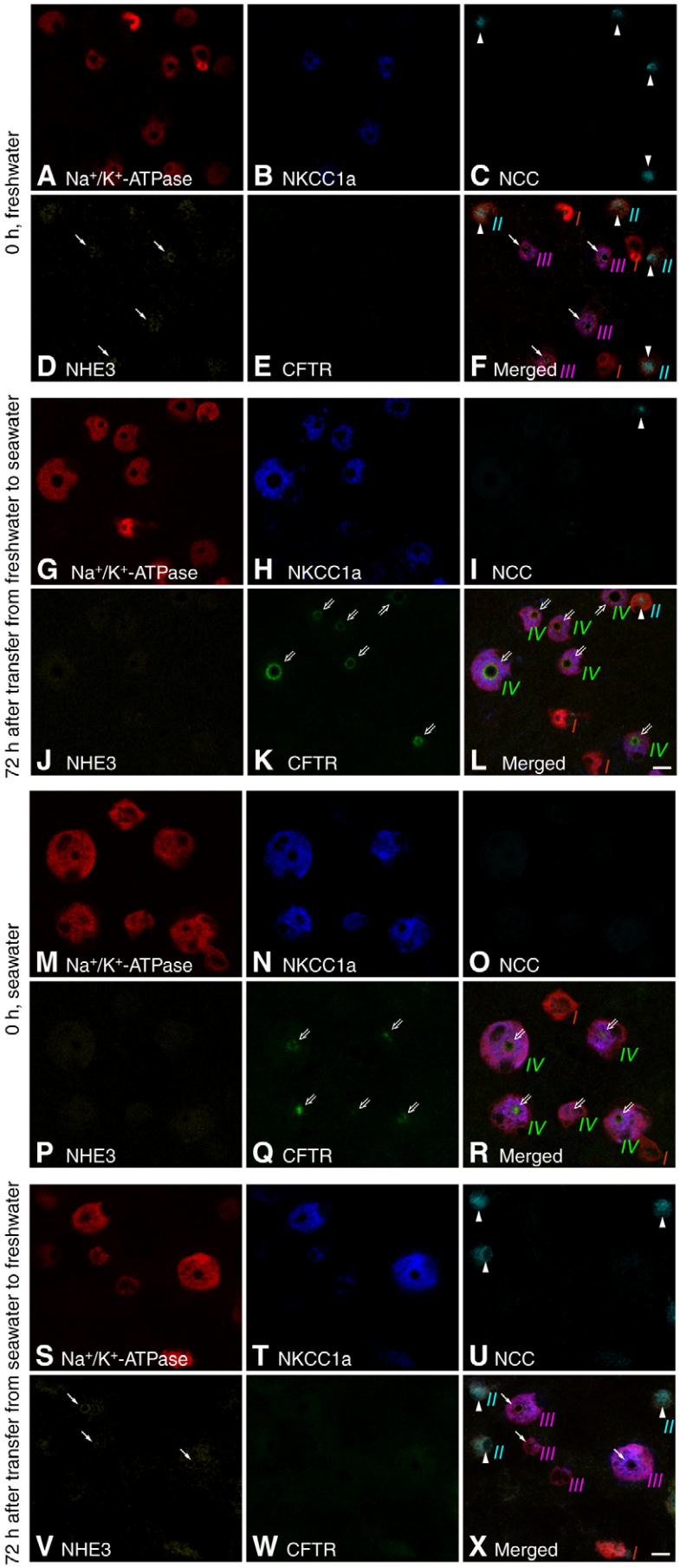

Fig. 8. Quintuple-color immunofluorescence staining for Na^+/K^+-ATPase (red), NKCC1a (blue), NCC (cyan), NHE3 (yellow) and CFTR (green), at (A–F) 0 h and (G–L) 72 h of the freshwater-to-seawater transfer experiment, and at (M–R) 0 h and (S–X) 72 h of the seawater-to-freshwater transfer experiment. Arrowheads, arrows and double-lined arrows indicate the apical immunoreactivity for NCC, NHE3 and CFTR, respectively. *I*, type-I mitochondria-rich cell (MRC); *II*, type-II MRC; *III*, type-III MRC; *IV*, type-IV MRC. Scale bar, 10 μm.

NKCC2 was found in both the kidney and intestine (Fig. 4C), whereas eel NKCC2α was restricted to the kidney and NKCC2β found in the intestine and urinary bladder (Cutler and Cramb, 2002). Tilapia NCC was restricted to the freshwater gills and yolk-sac membrane (Fig. 4D), whereas eel NCCα was found in the kidney, and NCCβ in the intestine (Cutler and Cramb, 2002). Thus, the tissue distribution patterns of NKCC1 isoforms seem likely to be conserved, but those of NKCC2 and NCC could vary among teleosts. It will be of great interest to study comparatively the cation–chloride cotransporter family genes and their expression patterns in euryhaline and stenohaline teleosts.

Immunolocalization of freshwater- and seawater-type cotransporters

Our second and more crucial objective was to obtain more-convincing evidence that NKCC1a and NCC are involved in ion secretion and absorption, respectively, by determining their localization patterns within tilapia MRCs at the protein level. We succeeded in generating antibodies specific for tilapia NKCC1a and tilapia NCC (Fig. 1) and performed whole-mount immunofluorescence staining on the embryonic yolk-sac membrane with antibodies against NKCC1a and NCC, together with antibodies against Na^+/K^+-ATPase, CFTR and NHE3. This simultaneous quintuple-color immunofluorescence staining revealed the apical or basolateral localizations of multiple ion-transport proteins at the single-cell level and consequently allowed us to classify MRCs clearly into four types – types I, II, III and IV (Table 3; Fig. 6) – and also to quantify changes in the number of each MRC type following transfer to different salinities (Figs 8 and 9). The same four types of MRC classification have already been accomplished in our previous study (Hiroi et al., 2005), by triple-color immunofluorescence staining with antibodies against human NKCC1, Na^+/K^+-ATPase and CFTR. However, we are now able to distinguish immunocytochemically between NKCC1a and NCC, which were not distinguishable in the previous study (the antibody against human NKCC1 reacts with both tilapia NKCC1a and tilapia NCC).

The NKCC1a immunoreactivity was localized to the basolateral membrane of type-IV MRCs (Fig. 6D). Type-IV MRCs were defined by basolateral Na^+/K^+-ATPase, basolateral NKCC1a and apical CFTR, and this distribution pattern was completely consistent with the current accepted model for ion secretion by MRCs in seawater (Evans et al., 2005). This cell type was purely seawater specific: the cells were not observable in freshwater, rapidly appeared

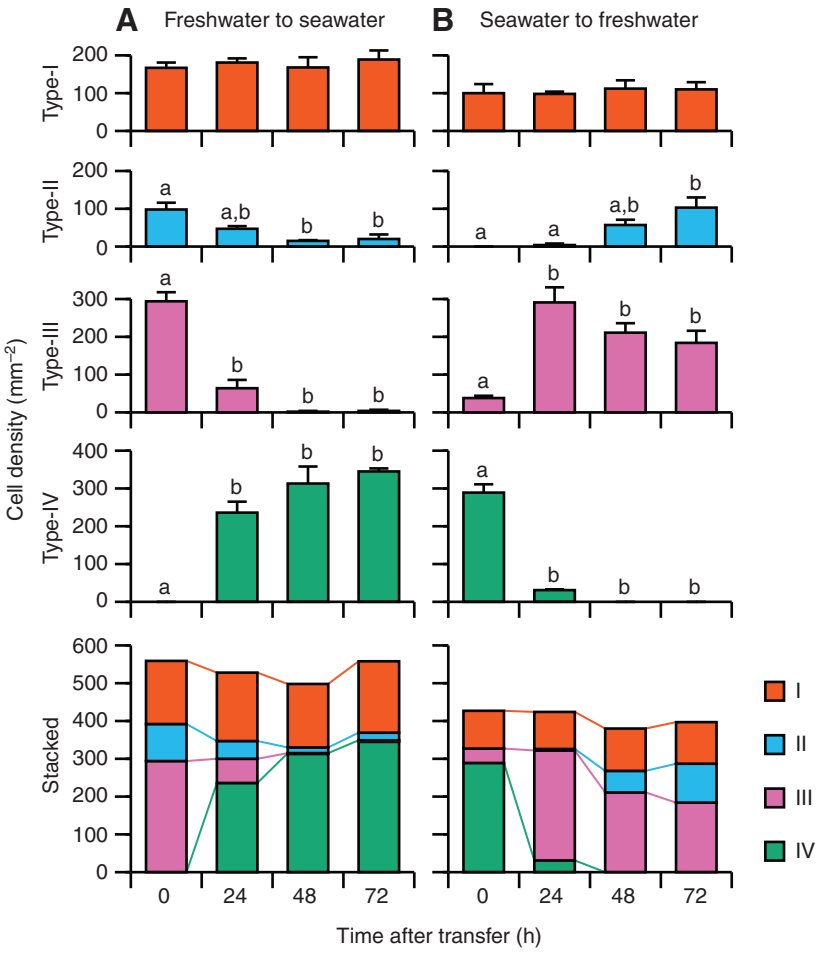

Fig. 9. Changes in the density of the four mitochondria-rich cell (MRC) types following transfer from (A) freshwater to seawater and (B) *vice versa*. Each value represents the mean ± s.e.m., *N*=5. Values with different lowercase letters are significantly different (*P*<0.0125, Tukey–Kramer test). Red, type-I MRC; cyan, type-II MRC; magenta, type-III MRC; green, type-IV MRC.

following transfer from freshwater to seawater and rapidly disappeared following transfer from seawater to freshwater (Fig. 9). From these facts, we deduce that type-IV MRCs are the seawater-type ion-secretory cells and that the NKCC1a protein localized at the basolateral membrane probably cotransports Na^+, K^+ and Cl^- from the internal environment into the cell.

The NCC immunoreactivity was restricted to the apical membrane of type-II MRCs and was not observable in other cell types (Fig. 6B). Accordingly, the immunoreactivity of NKCC1a and NCC was never colocalized to the same cell. Type-II MRCs were defined by apical NCC and basolateral Na^+/K^+-ATPase and showed freshwater-specific changes: they were absent in seawater, appeared following transfer from seawater to freshwater and decreased following transfer from freshwater to seawater (Fig. 9). Therefore, it seems likely that type-II MRCs are the freshwater-type ion-absorptive cells and that the apically located NCC protein should cotransport Na^+ and Cl^- from the external environment into the cell.

Proposal of a novel ion-uptake model utilizing NCC

Taking account of the presence of NCC-positive type-II MRCs in freshwater, we propose a novel model for active Na^+/Cl^- absorption by teleost MRCs in freshwater. The model consists of an apical NCC, basolateral Na^+/K^+-ATPase and basolateral Cl^- channel: Na^+ and Cl^- are cotransported by apical NCC from the external environment into the cell and then separately transported to the internal environment through a basolateral Na^+/K^+-ATPase and basolateral Cl^- channel, respectively. This model is depicted in the bottom row of Fig. 6B.

In order to establish the model, it will be necessary to determine the functional property of tilapia NCC as a Na^+/Cl^- cotransporter. We tentatively designated 'tilapia NCC' in accordance with its relatively high amino acid identity to human NCC (52.1%). However, in some teleosts (eel, zebrafish and medaka), several NCC isoforms were present, and the phylogenetic analysis suggested that they were divided into two clades, namely the conventional NCC clade and the fish-specific NCC clade (Fig. 3). Human NCC was assigned to the former clade, and tilapia NCC was assigned to the latter clade, and it would therefore be questionable whether tilapia NCC shows a functional property similar to that of human NCC. Thiazide-sensitive Na^+/Cl^- cotransport function was confirmed in human NCC and winter flounder NCC by using a *Xenopus laevis* oocyte expression system (Gamba et al., 1993; Gamba et al., 1994). We tried to assess the functional properties of tilapia NCC by using the same expression system but have not been successful (data not shown). However, in zebrafish, four NCC isoforms were identified; one of the four (zNCCg, EF591989), which was assigned to the fish-specific NCC clade, was expressed in MRCs of zebrafish embryos; knockdown of the translation of the MRC-specific NCC using morpholino antisense oligonucleotides impaired Cl^- uptake from freshwater (Y. F. Wang, Y. C. Tseng, J. J. Yan, J. Hiroi and P. P. Hwang, unpublished observations). Furthermore, in the gills of adult tilapia, mRNA encoding NCC was significantly upregulated in deionized water and low-Cl^- (but not low-Na^+) freshwater compared with normal freshwater (M. Inokuchi, J.H., S. Watanabe, K. M. Lee and T.K., unpublished observations). These preliminary data provide further evidence that NCC in MRCs is involved in ion uptake (at least Cl^-) from freshwater, strongly supporting the new model.

The Na^+/Cl^- cotransport system is electroneutral and therefore requires a driving force to cotransport Na^+ and Cl^- into the cell. One possible driving force would be an extremely low level of intracellular Na^+, which could be generated by basolaterally located Na^+/K^+-ATPase in type-II MRCs. Thus, a testable hypothesis of this model is that intracellular Na^+ will be low, at least in the apical region, of tilapia type-II MRCs. To transport Cl^- out of the cell, a Cl^- channel seems likely also to be required at the basolateral membrane, although its presence was not examined in this study. However, cDNAs encoding two Cl^- channels have been cloned from tilapia gills (OmCLC-3 and OmCLC-5) (Miyazaki et al., 1999), and ascertaining the basolateral localization of Cl^- channels within type-II MRCs will help clarify the new model.

Reevaluation of a traditional ion-uptake model with NHE3

In addition to cation–chloride cotransporters, we also quantified mRNAs encoding NHE3 and vacuolar-type H^+-ATPase, which are the components of the two currently proposed ion-uptake models.

The mRNA encoding NHE3 was expressed noticeably in the yolk-sac membrane and gills of freshwater-acclimatized fish (Fig. 4E), showed no significant change during transfer from freshwater to seawater (Fig. 5A) but was significantly upregulated following transfer from seawater to freshwater (Fig. 5B). By contrast, the H^+-ATPase mRNA was not highly expressed in the yolk-sac membrane and gills of freshwater-acclimatized fish (Fig. 4F), and no significant change was observed during both freshwater-to-seawater and seawater-to-freshwater transfer (Fig. 5A,B). These results indicate that NHE3, rather than H^+-ATPase, is possibly involved in active ion uptake in freshwater-acclimatized tilapia. The ion-uptake model incorporating an apical Na^+/H^+ exchanger was proposed originally but has been energetically questioned (Kirschner, 1983; Avella and Bornancin, 1989). Nevertheless, recent studies at both the mRNA and protein levels with Japanese dace (*Tribolodon hakonensis*), tilapia, zebrafish and even the elasmobranch Atlantic stingray (*Dasyatis sabina*) suggested that NHE3 is involved in active ion absorption by MRCs in freshwater, at least in those species (Hirata et al., 2003; Hirose et al., 2003; Choe et al., 2005; Yan et al., 2007; Watanabe et al., 2008).

Although the ion-uptake model with an apical H^+-ATPase and ENaC has received some experimental support (e.g. Galvez et al., 2002; Reid et al., 2003; Lin et al., 2006; Horng et al., 2007; Esaki et al., 2007), the localization of the H^+-ATPase protein varies greatly among fish species: immunolocalization of H^+-ATPase was found at the apical membrane of both pavement cells and MRCs of the rainbow trout *Oncorhynchus mykiss* (Wilson et al., 2000), at the apical membrane of one of the two MRC types in zebrafish (Lin et al., 2006), a diffuse cellular and more intense apical localization in MRCs of juvenile lamprey *Petromyzon marinus* (Reiz-Santos et al., 2008), at the basolateral membrane of one of the two MRC types in stingray (Piermarini and Evans, 2001), at the basolateral membrane of MRCs in killifish *Fundulus heteroclitus* (Katoh et al., 2003) and at the apical membrane of pavement cells but not in MRCs of tilapia embryos (Hiroi et al., 1998). Furthermore, fish ENaC has yet to be identified by molecular cloning or database searches of fish genomes, and the evidence for the existence of ENaC, or equivalent Na^+ channels, will be needed to confirm the H^+-ATPase–ENaC model (Hirose et al., 2003; Hwang and Lee, 2007).

'Type-III+IV' MRCs

By quintuple-color immunofluorescence staining, the NHE3 immunoreactivity was only observable at the apical membrane of type-III MRCs (Fig. 6C). Type-III MRCs were defined by basolateral Na^+/K^+-ATPase and basolateral NKCC1a and showed freshwater-specific changes: they rarely appeared in seawater, rapidly increased in number following transfer from seawater to freshwater and disappeared rapidly following transfer from freshwater to seawater (Fig. 9). The rapid appearances or disappearances of type-III MRCs were largely completed within 24 h following both freshwater-to-seawater and seawater-to-freshwater transfer, and was the opposite of the pattern observed for type-IV MRCs. This inverse salinity-induced relationship between type-III and type-IV MRCs was consistent with our previous observations (fig. 6 in Hiroi et al., 2005). We suspect that type-III and type-IV MRCs are transformed from one to the other: that is, type-III and type-IV MRCs have the same cell origin and are only counted as type-III or type-IV according to the lack or presence of apical CFTR, respectively. If this were not true, a very high rate of cellular turnover would have to occur within 24 h: one cell type would almost completely disappear and be replaced by another cell type within 24 h. However, we were not aware of such an excessive cellular turnover by immunocytochemical observations in both the present and previous studies (Hiroi et al., 2005). Furthermore, by observing *in vivo* sequential changes in individual MRCs of living tilapia embryos, we have previously demonstrated that most MRCs are able to survive following transfer from freshwater to seawater: 90% of preexisting MRCs remain at 24 h, and 76% of the cells remain at 96 h (Hiroi et al., 1999). The continuous existence of MRCs following transfer from seawater to freshwater was also confirmed by the same technique (J.H., unpublished observations). Therefore, we are convinced that type-III and type-IV MRCs simply represent the same cells without, or with, apical CFTR, respectively. Type-III MRCs do not seem likely to function as ion-secretory cells because of the lack of apical CFTR.

Based on the lack of CFTR and presence of NHE3 at the apical membrane, type-III MRCs seem not only to stop ion secretion but also to be involved in ion absorption through apical NHE3, suggesting that type-III+IV MRCs possess the plasticity to alter their ion-transport function between secretion and absorption. The apical NHE3 in type-III MRCs also suggests that the two independent ion-uptake mechanisms – NCC based and NHE3 based – are separately present in type-II and type-III MRCs, respectively. Further molecular, physiological and morphological experiments will be needed to certify the two ion-uptake mechanisms in these cell types.

Time-course correlation between mRNA data and MRC types

Temporal changes in the levels of mRNAs encoding NKCC1a, NCC and NHE3 (Fig. 5) and the number of the four MRC types (Fig. 9) were examined in parallel with a single brood of tilapia embryos at the same 24 h intervals. Immunolocalizations of NKCC1a, NCC and NHE3 were restricted within type-III+IV MRCs, type-II MRCs and type-III MRCs, respectively. Therefore, it is useful to correlate the mRNA data and the morphological data on MRC types during transfer experiments to elucidate further the function of these cell types and their specific ion-transport proteins.

Type-II MRC and NCC

Following transfer from freshwater to seawater, the mRNA encoding NCC decreased rapidly to an extremely low level (Fig. 5A), whereas type-II MRCs gradually decreased in number but were still present at 72 h (a cell indicated by an arrowhead in Fig. 8I,L; Fig. 9A). These results suggest that the NCC protein remains at the apical membrane of type-II MRCs following transfer from freshwater to seawater, although the NCC mRNA was quickly downregulated (the transcription would be stopped, and/or perhaps the mRNA was rapidly degraded). The remaining type-II MRCs at 72 h showed the distinct apical NCC immunoreactivity, but their apical membrane was isolated from the external environment by surface pavement cells (Fig. 7H–N). Therefore, the remaining type-II MRCs seem likely to stop ion absorption in seawater, but, when encountering freshwater again, they could rapidly resume ion absorption by contacting the external environment and using the existing apical NCC protein more quickly (rather than by synthesizing NCC *de novo*). This speculation seems to be reasonable, especially for euryhaline tilapia that have the capacity to live in unstable salinity environments.

During transfer from seawater to freshwater, mRNA encoding NCC was initially extremely low and then increased steadily and linearly (Fig. 5B). Type-II MRCs were not observed in seawater and appeared and increased in number steadily after transfer to freshwater (Fig. 9B). These changes imply that type-II MRCs arise from an undifferentiated cell type following transfer from seawater to freshwater, rather than transform from other

preexisting MRC types. The increase in the NCC mRNA and type-II MRCs during seawater-to-freshwater transfer was relatively slow compared with the quick response of the NKCC1a mRNA and type-III+IV MRCs during freshwater-to-seawater transfer. The ion absorption by type-II MRCs with NCC might be compensated by other ion-absorptive MRCs, such as type-III MRCs with NHE3. Furthermore, the necessity for rapid ion absorption in freshwater might be less urgent than that for ion secretion in seawater; although ion absorption is indispensable for fish to acclimatize to the hypotonic freshwater environment, the turnover rate of Na^+ and Cl^- in freshwater-acclimatized fish is markedly lower than in seawater-acclimatized fish (Potts et al., 1967; Maetz, 1974; Guggino, 1980). Indeed, the Cl^- turnover rate of tilapia embryos is 50–100 times lower in freshwater than in seawater (Miyazaki et al., 1998). Therefore, the slow increase in the NCC mRNA and type-II MRC number could be sufficient to meet the necessity for ion absorption in freshwater.

The NCC-positive apical opening of type-II MRCs was relatively small in embryos at 0 h of freshwater-to-seawater transfer (Fig. 7A–G; Fig. 8C,F) but was much larger in embryos at 72 h of seawater-to-freshwater transfer (Fig. 7V–AI; Fig. 8U,X). When embryos at 0 h in freshwater were not transferred to seawater but maintained in freshwater for 72 h, the relatively small apical opening was still observed (data not shown). The larger apical opening implies greater NCC protein abundance in type-II cells, and it therefore seems likely that embryos might be required to absorb more ions during acclimatization from seawater to freshwater than embryos developing throughout in freshwater.

Type-III+IV MRC and NKCC1a

Following transfer from freshwater to seawater, the mRNA encoding NKCC1a increased rapidly (Fig. 5A), and type-III MRCs quickly expressed apical CFTR, consequently counted as type-IV MRCs (Fig. 9A). This rapid NKCC1a mRNA increase seems to be attributable mainly to the upregulation of NKCC1a within preexisting type-III+IV MRCs and probably partly by the recruitment of newly differentiated type-III+IV MRCs. Each of the type-III+IV MRCs showed more-intense NKCC1a immunoreactivity and enlarged their cell size during the course of transfer (e.g. compare Fig. 8B,F and Fig. 8H,L), and both the increase in staining intensity and staining area for NKCC1a protein might explain the threefold-elevated expression of mRNA encoding NKCC1a in seawater. Although we did not measure the size of MRCs in this study, the enlargement of type-III+IV MRCs following transfer from freshwater to seawater could be demonstrated by the combination of our previous two studies: most of the MRCs not only survived but also grew larger according to *in vivo* sequential observations on individual MRCs (figs 2 and 3 in Hiroi et al., 1999); the average size of type-III+IV MRCs was significantly larger at 72 h than at 0 h (295 μm^2 and 210 μm^2, respectively), but the size was not changed significantly for type-I and type-II MRCs between 0 h and 72 h (fig. 7A in Hiroi et al., 2005).

Following transfer from seawater to freshwater, the NKCC1a mRNA was reduced relatively slowly (Fig. 5B). Type-IV MRCs quickly lost apical CFTR to be counted as type-III MRCs, and the sum of type-III and type-IV MRCs showed a slight decrease during transfer (Fig. 9B). The decrease in mRNA encoding NKCC1a indicates that NKCC1a was less necessary in freshwater, but a certain level of its expression in freshwater (one-third of the initial level in seawater) implies that NKCC1a could have some direct physiological function in freshwater (e.g. ion absorption, acid–base regulation or cell-volume regulation). The NKCC1a-immunopositive staining intensity and staining area showed little change during seawater-to-freshwater transfer, which was in contrast to the increase during freshwater-to-seawater transfer mentioned above: the type-III+IV MRCs showed strong NKCC1a immunoreactivity and were hypertrophied in seawater (at 0 h, Fig. 8N,R) and kept the strong immunoreactivity and the size after transfer to freshwater (Fig. 8T,X). Little change in the size of type-III+IV MRCs during seawater-to-freshwater transfer was also demonstrated by two observations: each of the hypertrophied MRCs maintained their size following transfer from seawater to freshwater as assessed by *in vivo* sequential observation (J.H., unpublished observations), and the average size of type-III+IV MRCs was 388 μm^2 at 0 h and 360 μm^2 at 72 h (fig. 7B in Hiroi et al., 2005). If transferred back to seawater, these remaining large type-III MRCs in freshwater are expected to be able to resume ion secretion by using the existing basolateral NKCC1a protein and the apical CFTR, which would be quickly synthesized *de novo*.

Type-III+IV MRC and NHE3

The level of mRNA encoding NHE3 was twofold higher in embryos developed throughout in freshwater than those in seawater (Fig. 4E; 0 h of Fig. 5A,B), did not change significantly during freshwater-to-seawater transfer (Fig. 5A) and increased significantly during seawater-to-freshwater transfer (Fig. 5B). Its higher level in freshwater and upregulation following transfer from seawater to freshwater implies that NHE3 is involved in ion absorption in freshwater. However, the levels of mRNA encoding NHE3 are still substantial in seawater, suggesting a physiological function such as acid–base regulation: the apically located Na^+/H^+ exchanger is considered to be involved in H^+ excretion to the external environment in both freshwater and seawater fish (see review by Claiborne et al., 2002). The apical NHE3 immunoreactivity was only observable in tilapia embryos at 0 h of freshwater-to-seawater transfer (Fig. 8D,F) and at 72 h of seawater-to-freshwater (Fig. 8V,X). However, MRCs in the gills of adult tilapia showed the apical NHE3 immunoreactivity in seawater as well as in freshwater (Watanabe et al., 2008; Inokuchi et al., in press). Therefore, it is possible that type-III+IV MRCs express apical NHE3 in seawater at a lower level than in freshwater, comparable to the ratio of its mRNA between freshwater and seawater, although we were not able to visualize it by the present immunocytochemical method.

Is type I an immature MRC?

Type-I MRCs showed only basolateral Na^+/K^+-ATPase (Fig. 6A) and appeared constantly during both the transfer experiments (Fig. 9A,B). Because of their relatively small size, possessing only Na^+/K^+-ATPase immunoreactivity, and relatively small apical opening, we had speculated that type-I MRCs were immature MRCs possessing the capacity to develop into other MRC types, especially type-II MRCs that appeared following transfer from seawater to freshwater (Hiroi et al., 2005). However, we are presently doubtful about this speculation. In the present study, we were not able to observe a transition from type-I to type-II MRCs throughout the transfer from seawater to freshwater. Instead, we often found small type-II MRCs at 24 h and 48 h; these small MRCs showed weak Na^+/K^+-ATPase immunoreactivity as well as weak and relatively diffuse NCC immunoreactivity (Fig. 7O–U) and were clearly distinguishable from type-I MRCs, which were characterized by rather strong and evenly stained Na^+/K^+-ATPase immunoreactivity. Therefore, these small type-II MRCs seem likely to newly arise following transfer from seawater to freshwater but not to transform from preexisting type-I MRCs.

Although type-I MRCs showed only Na^+/K^+-ATPase immunoreactivity, they might express other ion-transport proteins that were not examined in this study. One possibility is that type-I MRCs are involved in uptake of Ca^{2+}. A model for absorption of Ca^{2+} by fish MRCs consists of an apically located epithelial Ca^{2+} channel (ECaC), basolateral Ca^{2+}-ATPase, basolateral Na^+/Ca^{2+} exchanger and basolateral Na^+/K^+-ATPase (Flik et al., 1995). The cDNA encoding ECaC has been cloned in zebrafish and rainbow trout, and mRNA encoding ECaC was found in a portion of Na^+/K^+-ATPase-positive MRCs in developing zebrafish (Pan et al., 2005). ECaC immunoreactivity has been found in both pavement cells and Na^+/K^+-ATPase-positive MRCs of rainbow trout (Shahsavarani et al., 2006). Recently, we have cloned an ECaC homolog from tilapia gills and succeeded in generating a specific antibody showing apical immunoreactivity in gill MRCs (K. M. Lee and T.K., unpublished observations). We therefore hypothesize that the type-I MRC is not an immature cell but, rather, a functional ion-transport cell, possibly involved in transport of Ca^{2+}.

We are grateful to Professor Ichiro Iuchi, Director of Life Science Institute, Sophia University, for allowing J.H. to work there as a collaborative researcher and for his encouragement and stimulating discussions on molecular and phylogenetic studies. We thank Dr Hiroaki Miyazaki, Kyoto Prefectural University of Medicine, for his advice on molecular cloning and functional assays, Dr Mari Kawaguchi, Sophia University, for her advice on molecular cloning and phylogenetic analyses, Ms Kaoru Funatsu for her assistance in sampling of tilapia tissues, Ms Kayoko Suenaga, Carl Zeiss MicroImaging, for her technical help on confocal microscopy, and Dr Hajime Sakaguchi, Invitrogen, for his advice on choosing fluorescent dyes. We also thank Norra Co. for providing 'Micros Ceramic', which was used as filter media for tilapia brood-stock tanks. J.H. was supported in part by a Narishige Zoological Science Award, and Grant-in-Aid for Young Scientists (B) 17770055 and 20780147 from the Ministry of Education, Culture, Sports, Science and Technology of Japan.

LIST OF ABBREVIATIONS

ANOVA	analysis of variance
CFTR	cystic fibrosis transmembrane conductance regulator
ECaC	epithelial Ca^{2+} channel
ENaC	epithelial Na^+ channel
KCC	K^+/Cl^- cotransporter
MRC	mitochondria-rich cell
NCC	Na^+/Cl^- cotransporter
NHE	Na^+/H^+ exchanger
NKCC	$Na^+/K^+/2Cl^-$ cotransporter
SLC	solute carrier family

REFERENCES

Avella, M. and Bornancin, M. (1989). A new analysis of ammonia and sodium transport through the gills of the freshwater rainbow trout (*Salmo gairdneri*). *J. Exp. Biol.* **142**, 155-175.

Choe, K. P., Kato, A., Hirose, S., Plata, C., Sindic, A., Romero, M. F., Claiborne, J. B. and Evans, D. H. (2005). NHE3 in an ancestral vertebrate: primary sequence, distribution, localization, and function in gills. *Am. J. Physiol. Regul. Integr. Comp. Physiol.* **289**, R1520-R1534.

Claiborne, J. B., Edwards, S. L. and Morrison-Shetlar, A. I. (2002). Acid-base regulation in fishes: cellular and molecular mechanisms. *J. Exp. Zool.* **293**, 302-319.

Cutler, C. P. and Cramb, G. (2002). Two isoforms of the $Na^+/K^+/2Cl^-$ cotransporter are expressed in the European eel (*Anguilla anguilla*). *Biochim. Biophys. Acta* **1566**, 92-103.

Cutler, C. P. and Cramb, G. (2008). Differential expression of absorptive cation-chloride-cotransporters in the intestinal and renal tissues of the European eel (*Anguilla anguilla*). *Comp. Biochem. Physiol.* **149B**, 63-73.

Esaki, M., Hoshijima, K., Kobayashi, S., Fukuda, H., Kawakami, K. and Hirose, S. (2007). Visualization in zebrafish larvae of Na^+ uptake in mitochondria-rich cells whose differentiation is dependent on foxi3a. *Am. J. Physiol. Regul. Integr. Comp. Physiol.* **292**, R470-R480.

Evans, D. H., Piermarini, P. M. and Choe, K. P. (2005). The multifunctional fish gill: dominant site of gas exchange, osmoregulation, acid-base regulation, and excretion of nitrogenous waste. *Physiol. Rev.* **85**, 97-177.

Felsenstein, J. (1985). Confidence limits on phylogenies: an approach using the bootstrap. *Evolution* **39**, 783-791.

Flik, G., Verbost, P. M. and Wendelaar Bonga, S. E. (1995). Calcium transport processes in fishes. In *Fish Physiology*. Vol. 14 (ed. C. M. Wood and T. J. Shuttleworth), pp. 317-342. San Diego: Academic Press.

Galvez, F., Reid, S. D., Hawkings, G. and Goss, G. G. (2002). Isolation and characterization of mitochondria-rich cell types from the gill of freshwater rainbow trout. *Am. J. Physiol. Regul. Integr. Comp. Physiol.* **282**, R658-R668.

Gamba, G. (2005). Molecular physiology and pathophysiology of electroneutral cation-chloride cotransporters. *Physiol. Rev.* **85**, 423-493.

Gamba, G., Saltzberg, S. N., Lombardi, M., Miyanoshita, A., Lytton, J., Hediger, M. A., Brenner, B. M. and Hebert, S. C. (1993). Primary structure and functional expression of a cDNA encoding the thiazide-sensitive, electroneutral sodium-chloride cotransporter. *Proc. Natl. Acad. Sci. USA* **90**, 2749-2753.

Gamba, G., Miyanoshita, A., Lombardi, M., Lytton, J., Lee, W. S., Hediger, M. A. and Hebert, S. C. (1994). Molecular cloning, primary structure, and characterization of two members of the mammalian electroneutral sodium-(potassium)-chloride cotransporter family expressed in kidney. *J. Biol. Chem.* **269**, 17713-17722.

Geck, P., Pietrzyk, C., Burckhardt, B. C., Pfeiffer, B. and Heinz, E. (1980). Electrically silent cotransport on Na^+, K^+ and Cl^- in Ehrlich cells. *Biochim. Biophys. Acta* **600**, 432-447.

Gerelsaikhan, T. and Turner, R. J. (2000). Transmembrane topology of the secretory Na^+-K^+-$2Cl^-$ cotransporter NKCC1 studied by *in vitro* translation. *J. Biol. Chem.* **275**, 40471-40477.

Guggino, W. B. (1980). Salt balance in embryos of *Fundulus heteroclitus* and *F. bermudae* adapted to seawater. *Am. J. Physiol.* **238**, R42-R49.

Hebert, S. C., Mount, D. B. and Gamba, G. (2004). Molecular physiology of cation-coupled Cl^- cotransport: the SLC12 family. *Pflugers Arch.* **447**, 580-593.

Hirata, T., Kaneko, T., Ono, T., Nakazato, T., Furukawa, N., Hasegawa, S., Wakabayashi, S., Shigekawa, M., Chang, M. H., Romero, M. F. et al. (2003). Mechanism of acid adaptation of a fish living in a pH 3.5 lake. *Am. J. Physiol. Regul. Integr. Comp. Physiol.* **284**, R1199-R1212.

Hiroi, J. and McCormick, S. D. (2007). Variation in salinity tolerance, gill Na^+/K^+-ATPase, $Na^+/K^+/2Cl^-$ cotransporter and mitochondria-rich cell distribution in three salmonids *Salvelinus namaycush*, *Salvelinus fontinalis* and *Salmo salar*. *J. Exp. Biol.* **210**, 1015-1024.

Hiroi, J., Kaneko, T., Uchida, K., Hasegawa, S. and Tanaka, M. (1998). Immunolocalization of vacuolar-type H^+-ATPase in the yolk-sac membrane of tilapia (*Oreochromis mossambicus*) larvae. *Zool. Sci.* **15**, 447-453.

Hiroi, J., Kaneko, T. and Tanaka, M. (1999). *In vivo* sequential changes in chloride cell morphology in the yolk-sac membrane of Mozambique tilapia (*Oreochromis mossambicus*) embryos and larvae during seawater adaptation. *J. Exp. Biol.* **202**, 3485-3495.

Hiroi, J., McCormick, S. D., Ohtani-Kaneko, R. and Kaneko, T. (2005). Functional classification of mitochondrion-rich cells in euryhaline Mozambique tilapia (*Oreochromis mossambicus*) embryos, by means of triple immunofluorescence staining for Na^+/K^+-ATPase, $Na^+/K^+/2Cl^-$ cotransporter and CFTR anion channel. *J. Exp. Biol.* **208**, 2023-2036.

Hirose, S., Kaneko, T., Naito, N. and Takei, Y. (2003). Molecular biology of major components of chloride cells. *Comp. Biochem. Physiol.* **136B**, 593-620.

Horng, J. L., Lin, L. Y., Huang, C. J., Katoh, F., Kaneko, T. and Hwang, P. P. (2007). Knockdown of V-ATPase subunit A (atp6v1a) impairs acid secretion and ion balance in zebrafish (*Danio rerio*). *Am. J. Physiol. Regul. Integr. Comp. Physiol.* **292**, R2068-R2076.

Hwang, P. P. and Lee, T. H. (2007). New insights into fish ion regulation and mitochondrion-rich cells. *Comp. Biochem. Physiol.* **148A**, 479-497.

Inokuchi, M., Hiroi, J., Watanabe, S., Lee, K. M. and Kaneko, T. (in press). Gene expression and morphological localization of NHE3, NCC and NKCC1a in branchial mitochondria-rich cells of Mozambique tilapia (*Oreochromis mossambicus*) acclimated to a wide range of salinities. *Comp. Biochem. Physiol. A.*

Jentsch, T. J., Hubner, C. A. and Fuhrmann, J. C. (2004). Ion channels: function unravelled by dysfunction. *Nat. Cell. Biol.* **6**, 1039-1047.

Kaneko, T. and Hiroi, J. (2008). Osmo- and ionoregulation. In *Fish Larval Physiology* (ed. R. N. Finn and B. G. Kapoor), pp. 163-183. Enfield, NH, USA: Science Publishers.

Kaneko, T., Shiraishi, K., Katoh, F., Hasegawa, S. and Hiroi, J. (2002). Chloride cells during early life stages of fish and their functional differentiation. *Fish. Sci.* **68**, 1-9.

Kasahara, M., Naruse, K., Sasaki, S., Nakatani, Y., Qu, W., Ahsan, B., Yamada, T., Nagayasu, Y., Doi, K., Kasai, Y. et al. (2007). The medaka draft genome and insights into vertebrate genome evolution. *Nature* **447**, 714-719.

Katoh, F. and Kaneko, T. (2003). Short-term transformation and long-term replacement of branchial chloride cells in killifish transferred from seawater to freshwater, revealed by morphofunctional observations and a newly established 'time-differential double fluorescent staining' technique. *J. Exp. Biol.* **206**, 4113-4123.

Katoh, F., Shimizu, A., Uchida, K. and Kaneko, T. (2000). Shift of chloride cell distribution during early life stages in seawater-adapted killifish, *Fundulus heteroclitus*. *Zool. Sci.* **17**, 11-18.

Katoh, F., Hyodo, S. and Kaneko, T. (2003). Vacuolar-type proton pump in the basolateral plasma membrane energizes ion uptake in branchial mitochondria-rich cells of killifish *Fundulus heteroclitus*, adapted to a low ion environment. *J. Exp. Biol.* **206**, 793-803.

Kirschner, L. B. (1983). Sodium chloride absorption across the body surface: frog skins and other epithelia. *Am. J. Physiol.* **244**, R429-R443.

Kirschner, L. B. (2004). The mechanism of sodium chloride uptake in hyperregulating aquatic animals. *J. Exp. Biol.* **207**, 1439-1452.

Lin, L. Y., Horng, J. L., Kunkel, J. G. and Hwang, P. P. (2006). Proton pump-rich cell secretes acid in skin of zebrafish larvae. *Am. J. Physiol. Cell. Physiol.* **290**, C371-C378.

Luquet, C. M., Weihrauch, D., Senek, M. and Towle, D. W. (2005). Induction of branchial ion transporter mRNA expression during acclimation to salinity change in the euryhaline crab *Chasmagnathus granulatus*. *J. Exp. Biol.* **208**, 3627-3636.

Lytle, C., Xu, J. C., Biemesderfer, D. and Forbush, B., III. (1995). Distribution and diversity of Na-K-Cl cotransport proteins: a study with monoclonal antibodies. *Am. J. Physiol.* **269**, C1496-C1505.

Maetz, J. (1974). Aspects of adaptation to hypo-osmotic and hyper-osmotic environments. In *Biochemical and Biophysical Perspectives in Marine Biology*. Vol. 1 (ed. D. C. Malins and J. R. Sargent), pp. 1-167. San Diego: Academic Press.
Marshall, W. S. (2002). Na^+, Cl^-, Ca^{2+} and Zn^{2+} transport by fish gills: retrospective review and prospective synthesis. *J. Exp. Zool.* **293**, 264-283.
Marshall, W. S., Lynch, E. M. and Cozzi, R. R. (2002). Redistribution of immunofluorescence of CFTR anion channel and NKCC cotransporter in chloride cells during adaptation of the killifish *Fundulus heteroclitus* to sea water. *J. Exp. Biol.* **205**, 1265-1273.
McCormick, S. D., Sundell, K., Bjornsson, B. T., Brown, C. L. and Hiroi, J. (2003). Influence of salinity on the localization of Na^+/K^+-ATPase, $Na^+/K^+/2Cl^-$ cotransporter (NKCC) and CFTR anion channel in chloride cells of the Hawaiian goby (*Stenogobius hawaiiensis*). *J. Exp. Biol.* **206**, 4575-4583.
Miyazaki, H., Kaneko, T., Hasegawa, S. and Hirano, T. (1998). Developmental changes in drinking rate and ion and water permeability during early life stages of euryhaline tilapia, *Oreochromis mossambicus*, reared in fresh water and seawater. *Fish Physiol. Biochem.* **18**, 277-284.
Miyazaki, H., Uchida, S., Takei, Y., Hirano, T., Marumo, F. and Sasaki, S. (1999). Molecular cloning of CLC chloride channels in *Oreochromis mossambicus* and their functional complementation of yeast CLC gene mutant. *Biochem. Biophys. Res. Commun.* **255**, 175-181.
Pan, T. C., Liao, B. K., Huang, C. J., Lin, L. Y. and Hwang, P. P. (2005). Epithelial Ca^{2+} channel expression and Ca^{2+} uptake in developing zebrafish. *Am. J. Physiol. Regul. Integr. Comp. Physiol.* **289**, R1202-R1211.
Pelis, R. M., Zydlewski, J. and McCormick, S. D. (2001). Gill Na^+-K^+-$2Cl^-$ cotransporter abundance and location in Atlantic salmon: effects of seawater and smolting. *Am. J. Physiol. Regul. Integr. Comp. Physiol.* **280**, R1844-R1852.
Perry, S. F., Shahsavarani, A., Georgalis, T., Bayaa, M., Furimsky, M. and Thomas, S. L. (2003). Channels, pumps, and exchangers in the gill and kidney of freshwater fishes: their role in ionic and acid-base regulation. *J. Exp. Zool.* **300**, 53-62.
Piermarini, P. M. and Evans, D. H. (2001). Immunochemical analysis of the vacuolar proton-ATPase B-subunit in the gills of a euryhaline stingray (*Dasyatis sabina*): effects of salinity and relation to Na^+/K^+-ATPase. *J. Exp. Biol.* **204**, 3251-3259.
Potts, W. T., Foster, M. A., Rudy, P. P. and Howells, G. P. (1967). Sodium and water balance in the cichlid teleost, *Tilapia mossambica*. *J. Exp. Biol.* **47**, 461-470.
Reid, S. D., Hawkings, G. S., Galvez, F. and Goss, G. G. (2003). Localization and characterization of phenamil-sensitive Na^+ influx in isolated rainbow trout gill epithelial cells. *J. Exp. Biol.* **206**, 551-559.
Reis-Santos, P., McCormick, S. D. and Wilson, J. M. (2008). Ionoregulatory changes during metamorphosis and salinity exposure of juvenile sea lamprey (*Petromyzon marinus* L.). *J. Exp. Biol.* **211**, 978-988.
Riestenpatt, S., Onken, H. and Siebers, D. (1996). Active absorption of Na^+ and Cl^- across the gill epithelium of the shore crab *Carcinus maenas*: voltage-clamp and ion-flux studies. *J. Exp. Biol.* **199**, 1545-1554.
Saitou, N. and Nei, M. (1987). The neighbor-joining method: a new method for reconstructing phylogenetic trees. *Mol. Biol. Evol.* **4**, 406-425.
Shahsavarani, A., McNeill, B., Galvez, F., Wood, C. M., Goss, G. G., Hwang, P. P. and Perry, S. F. (2006). Characterization of a branchial epithelial calcium channel (ECaC) in freshwater rainbow trout (*Oncorhynchus mykiss*). *J. Exp. Biol.* **209**, 1928-1943.
Silva, P., Solomon, R., Spokes, K. and Epstein, F. (1977). Ouabain inhibition of gill Na-K-ATPase: relationship to active chloride transport. *J. Exp. Zool.* **199**, 419-426.
Thompson, J. D., Higgins, D. G. and Gibson, T. J. (1994). CLUSTAL W: improving the sensitivity of progressive multiple sequence alignment through sequence weighting, position-specific gap penalties and weight matrix choice. *Nucleic Acids Res.* **22**, 4673-4680.
Watanabe, S., Niida, M., Maruyama, T. and Kaneko, T. (2008). Na^+/H^+ exchanger isoform 3 expressed in apical membrane of gill mitochondrion-rich cells in Mozambique tilapia *Oreochromis mossambicus*. *Fish. Sci.* **74**, 813-821.
Wilson, J. M., Laurent, P., Tufts, B. L., Benos, D. J., Donowitz, M., Vogl, A. W. and Randall, D. J. (2000). NaCl uptake by the branchial epithelium in freshwater teleost fish: an immunological approach to ion-transport protein localization. *J. Exp. Biol.* **203**, 2279-2296.
Wilson, J. M., Antunes, J. C., Bouça, P. D. and Coimbra, J. (2004). Osmoregulatory plasticity of the glass eel of *Anguilla anguilla*: freshwater entry and changes in branchial ion-transport protein expression. *Can. J. Fish. Aquat. Sci.* **61**, 432-442.
Wu, Y. C., Lin, L. Y. and Lee, T. H. (2003). Na^+,K^+,$2Cl^-$-cotransporter: a novel marker for identifying freshwater- and seawater-type mitochondria-rich cells in gills of the euryhaline tilapia, *Oreochromis mossambicus*. *Zool. Stud.* **42**, 186-192.
Xu, J. C., Lytle, C., Zhu, T. T., Payne, J. A., Benz, E., Jr and Forbush, B., III. (1994). Molecular cloning and functional expression of the bumetanide-sensitive Na-K-Cl cotransporter. *Proc. Natl. Acad. Sci. USA* **91**, 2201-2205.
Yan, J. J., Chou, M. Y., Kaneko, T. and Hwang, P. P. (2007). Gene expression of Na^+/H^+ exchanger in zebrafish H^+-ATPase-rich cells during acclimation to low-Na^+ and acidic environments. *Am. J. Physiol. Cell. Physiol.* **293**, C1814-C1823.
Zar, J. H. (1999). *Biostatistical Analysis*. 4th edn. Upper Saddle River: Prentice-Hall.